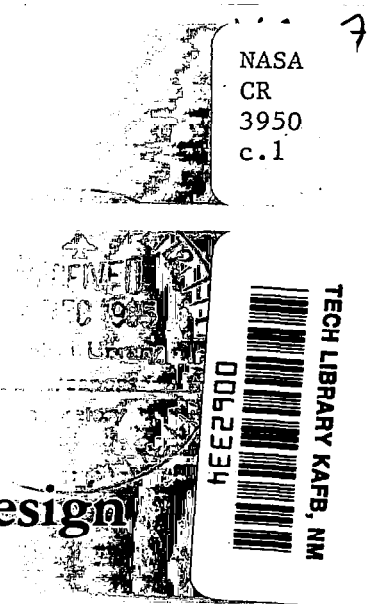

NASA Contractor Report 3950

Nonlinear Aerodynamic Wing Design

Ellwood Bonner

CONTRACT NAS1-15820
DECEMBER 1985

NASA

NASA Contractor Report 3950

Nonlinear Aerodynamic Wing Design

Ellwood Bonner
North American Aircraft Operations
Rockwell International Corporation
Los Angeles, California

Prepared for
Langley Research Center
under Contract NAS1-15820

National Aeronautics
and Space Administration

**Scientific and Technical
Information Branch**

1985

TABLE OF CONTENTS

LIST OF ILLUSTRATIONS

NOMENCLATURE

General Symbols

Aw	Wetted area, ft^2
AR	Aspect ratio, b^2/S
b	Wing span, ft
c	Chord, ft
$\bar{c}$	Mean aerodynamic chord, ft
C_d	Sectional drag coefficient, d/qc
C_D	Drag coefficient, D/qS
C_F	Average skin friction coefficient
C_ℓ	Sectional lift coefficient, ℓ/qc
C_L	Lift coefficient, L/qS
C_{L_α}	Lift curve slope, $dC_L/d\alpha$, per radian
C_M	Pitching moment coefficient $M/q\bar{c}S$
C_P	Pressure Coefficient
L/D	Lift to drag ratio
m	Mass flow rate, slugs/sec
M	Mach number
P_t	Total pressure, lb/ft^2
q	Dynamic pressure, lb/ft^2
$R_{n_{\bar{c}}}$	Reynolds number, $u\bar{c}/\nu$
S	Gross trapezoidal reference area, ft^2
S_c	Inlet capture area, ft^2
T_t	Total temperature, deg R
t/c	Thickness Ratio
x,y,z	Cartesian body axis; axial, lateral, vertical coordinates, ft

u	Freestream velocity, ft/sec
α	Angle of attack, deg
δ	Streamwise deflection angle, deg
δ^*	Boundary layer displacement thickness, ft
ε	Duct incidence angle in pitch, deg
η	Span station, 2y/b
Θ	Twist angle, deg
μ	Mach angle, deg
λ	Taper ratio
Λ	Sweep angle, deg
ν	Kinematic viscosity, ft^2/sec

Subscripts

avg	Average
c	Camber or chord
D	Design
F	Friction
i	Internal
L	Lift
LE	Leading edge
p	Pressure
t	Tip or thickness
r	Root
w	Wave
∞	Free stream

INTRODUCTION

The development and validation of advanced aerodynamic prediction techniques is required to support conceptual vehicle definition and optimization efforts since this is the design stage which has the greatest impact on subsequent system development.

Linear theory has been and currently still is widely used for such efforts. It is increasingly clear that limitations associated with this approximation are inhibiting advancement in supersonic aerodynamic performance state-of-the-art. In particular, embedded shock capture and management which has been crucial to transonic flow advancements has not been realized for practical three dimensional arrangements at supersonic conditions until very recently under other tasks of this contract. Further, nonlinear compressibility effects for transonic edge conditions remove spurious linear peaks that have heretofore excluded this design space from being exploited or for that matter even systematically examined.

Nonlinear irrotational (i.e., potential) approximations include enough physics of the flow to allow realistic optimization and permit consideration of component interactions of promising highly integrated arrangements. Such concepts have been the key to increasing aerodynamic efficiency using linear methodology. This approach in conjunction with the use of modern high speed computers achieves the objective of economic computational design that is responsive to conceptual aircraft development efforts. A demonstration of this capability is required to give impetus to its timely introduction into standard numerical aerodynamic design practice.

DISCUSSION

APPROACH

Linear theory[1,2] is used to establish candidate optimum thickness and zero suction drag due to lift, twist, camber, and variable camber deflections. Nonlinear potential flow analysis is employed to capture embedded shock waves at transonic[3,4] and supersonic conditions[5] and weaken the wave system through parametric redesign. Boundary layer analysis[6] is subsequently used to assess the flow quality of the nonlinear potential design. The extent of trailing edge separation in particular is evaluated. The general approach is schematically indicated on figure 1 and represents a summary of the numerical design experience at Rockwell covering the HiMAT, forward swept wing, SAAB, and Air Force/Navy Research Technology contract studies.[7-10]

A two point design cycle employing the previously described approach is illustrated on figure 2. The various steps for a supersonic cruise and transonic maneuver aerodynamic development problem are indicated on the left and right sides of the figure, respectively. The variable geometry system typically consists of deflectable leading and trailing edge flaps and aeroelastic twist. The steps above the dashed line use linear potential theory optimization while those below use nonlinear potential theory shock capture and pressure gradient management steps to maximize the extent of attached flow. The intent is to satisfy necessary far field and sufficient near field aerodynamic efficiency conditions, respectively. In general, an effective

compromise accepts limited trailing edge separation at the subsonic/transonic maneuver condition.

The specific aerodynamic methodology used for the present study is summarized on figure 3. It consists of three basic elements:

1. linear finite element theory[1,2]
2. nonlinear small pertubation[3] and full potential transonic[4] and supersonic[5] analysis
3. three dimensional finite difference boundary layer analysis[6].

The generic function of these elements is indicated. Their specific role in the present effort has already been described.

GENERAL ARRANGEMENT

The existing conceptual arrangement of figure 4 which was developed and sized to meet modern advanced tactical fighter requirements is used as a starting point for the present study. It consists of a blended (in both planform and cross section) wing body with widely spaced underslung nacelles and twin vertical tails. It incorporates an aspect ratio 3.0, leading edge sweep 48 degrees, taper ratio 0.2 reference trapezoidal planform wing, with a NACA 64A004 airfoil section for the outboard panel. The aerodynamic concept was developed to achieve high supersonic volumetric efficiency and meet transonic maneuver requirements through use of relatively high wing loading. The planform is consequently a compromise which requires advanced aerodynamic technology to develop an optimum camber surface.

SUPERSONIC POINT DESIGN

A configuration derivative was established in the present study to assess the impact of multipoint design compromises on the aerodynamic performance of a representative advanced tactical fighter and to validate the supersonic nonlinear potential analysis developed under other contract tasks.

The nominal design cycle used for the development of the uncompromised supersonic point design wing panel is presented on figure 5 and consists of a candidate arrangement definition, small disturbance linear optimization, full potential evaluation/refinement, and finite difference boundary layer assessment of the resulting inviscid flow. This procedure corresponds to progressing from left to right on figure 1 for a specific design point and employs fixed as opposed to variable wing geometry.

A 55-degree leading edge sweep outboard wing panel derivative was derived by axial shearing of the baseline planform to provide a 3.6 degrees subsonic edge condition at the design Mach number of 1.6. A revised inboard blending was developed to maintain smooth area progression and transition into the outboard panel. An overlay of the point design planform and the baseline is presented on figure 6. The NACA 64A004 airfoil section was retained for the present development.

A comparison of the drag due to thickness of the two cases is presented on figure 7. The arrows indicate a sonic leading edge condition that typically corresponds to linear theory peaks whose magnitude is related to the square of the thickness ratio. For the present case, the overall arrangement has high volumetric efficiency (i.e., low wave drag) and consequently small

sonic peaks. The impact of sweep is modest but favors the subsonic edge as expected.

The linear theory finite element optimization model of figure 8 was developed for the point design arrangement. Zero suction drag due to lift minimization[2] was performed for the outer wing panel ($2y/b > 0.375$) for a typical supersonic maneuvering condition of $M = 1.6$, $C_L = 0.32$. This spanwise limit or constraint is imposed due to the planned use of an existing high speed force model for the experimental phase of the study. The results are presented on figure 9 and compared to drag due to lift levels of a flat plate and a totally unconstrained optimum for the entire planform. The constrained optimum result is equivalent to full (100 percent) theoretical leading edge suction levels for a flat plate of the same gross planform. An examination of the spanwise drag variation presented on figure 10 indicates the design incurs penalities relative to the unconstrained case in the inboard region (i.e., $2y/b < 0.375$). A number of less spanwise constrained optimizations were subsequently performed in an effort to more closely approach the lower bound case. The resulting twists and cambers were impractical. Imposing twist smoothness still resulted in irregular cambers. Smoothing of the spanwise variation of camber resulted in drag due to lift levels approaching the initial constrained case of figure 9. Therefore, this case was selected to provide a well initialized model for subsequent nonlinear potential analysis refinement. The candidate twist and camber resulting from the optimization is presented on figure 11. The angle of attack for the configuration to develop a C_L of 0.32 was 4.46 degrees.

Full potential analysis[5] of the supersonic maneuver point design candidate was subsequently conducted. The geometric model of the wing-body/sting housing/vertical tails is presented on figure 12. A typical marching plane

57 x 20 mesh generated by the elliptic grid solver is indicated. Solution axial step size of 0.3 percent of total length was used to generate the surface pressure solution of figure 13. The canopy compression at the plane of symmetry is clearly visible and is followed by a second compression associated with the emergence of the sting housing. The outboard panel upper surface pressures are well behaved in the leading edge region and exhibit no cross-flow shocks. A swept compression region emanating from the forward inboard constrained region and terminating at the outboard trailing edge exists. This behavior is more evident from the isobar results. Three dimensional finite difference boundary layer evaluation[6] was conducted for the proposed test condition of $R_{n_{\bar{c}}} = 1.56 \times 10^6$. Transition was fixed at 2.5 percent chord and is consistent with the planned test trips. The wing upper surface normalized displacement thickness (δ^*/c) contours and wall shear stress vectors are presented on figure 14. The indicated swept displacement thickness ridge corresponds to the previously described swept compression region. Although the local wall flow direction is turned outboard (which is indicative of approaching separation) traversing this region, it remains fully attached to the trailing edge. Similar analysis for the lower surface indicated an orderly growth of displacement thickness and a fully attached flow. This is as expected based on the passive nature of the lower surface pressure distribution of figure 13. The conclusion is that linear optimization provided a nonlinear initialization candidate for the supersonic maneuver point design that met sufficient aerodynamic performance requirements and consequently was not refined.

Linear finite element and full potential estimates of the supersonic point design maneuver efficiency are presented on figure 15. Fully turbulent skin friction drag for a mean aerodynamic chord Reynolds number of 1.56×10^6 is used for this assessment and corresponds to the proposed nominal test condition for the Langley Unitary Plan Wind Tunnel. Examination of the results indicates the design is aerodynamically efficient, taking into consideration nominal scale effects.

MULTIPOINT WING DESIGN

A tactical aircraft must typically operate efficiently at subsonic, transonic, and supersonic speeds over a range of lift coefficient covering cruise through sustained/instantaneous maneuver conditions.

The following conditions were explicitly considered for the present development:

M_∞	C_L	Design Point
0.5	1.13	subsonic maneuver
0.9	0.80	transonic maneuver
1.6	0.1	supersonic cruise
1.6	0.32	supersonic maneuver

and correspond to representative subsonic/transonic maneuver and supersonic cruise/maneuver conditions. Linear theory zero suction camber drag was also monitored at $C_L = 0.1$ for $M_\infty = 0.6$, 0.9, 1.4, and 1.5 in addition to the previous design points.

The development cycle of figure 16 is used for the effort. Changes relative to the previously described supersonic point design will be initially described followed by variable geometry considerations incorporated to provide camber/twist management over the broad band of operating lift coefficient that must be addressed.

The effect of the transonic planform sweep compromise from 55 to 48 degrees on volumetric efficiency is presented on figure 17. A 3.3-degree supersonic leading edge exists at the design Mach number of 1.6. Sonic edge conditions are indicated by the arrows and correspond to linear theory peaks associated with such conditions. The NACA 64A004 section utilized for the supersonic point design outboard panel was modified for the multipoint wing based on Rockwell test results to incorporate a larger leading edge radius in order to achieve increased leading edge suction at subsonic conditions. A comparison of the two sections is presented on figure 18. The impact on wave drag is indicated on figure 17 and accentuates the previously found peak.

Based on Rockwell subsonic/transonic test results, spar box camber and twist was increased in the outboard wing panel to improve high C_L aerodynamic efficiency. The resulting camber has an unfavorable supersonic cruise impact which is offset by increased wing elasticity as much as possible. The baseline (i.e., undeflected) camber is presented on figure 19. Structural twist status for optimum ply orientation is also shown. The result considers substructure, fuselage elasticity, and employs maneuver load control. A nominal 3.75 degree tip twist increment exists between cruise and maneuver conditions.

The basic variable geometry philosophy used here is to configure the outboard wing for best aerodynamic performance without compromising for trim. This latter function is provided by the deflectable tail, body flap (wing trailing edge inboard of nacelle) and two dimensional vectorable nozzle. The use of an unstable low speed balance augments this objective by: a) allowing trim with wing trailing edge down deflection (favorable cambering) at subsonic and transonic speeds and b) reducing out of trim pitching moment at supersonic conditions.

The deflectable leading edge device employed two 12.5 percent chord geared (2/1) segments. The deflectable trailing edge utilized a conventional 25 percent chord plain flap. Both devices start at 37.5 percent span and were split at 66 percent span. The variable camber system definition is summarized in the following sketch.

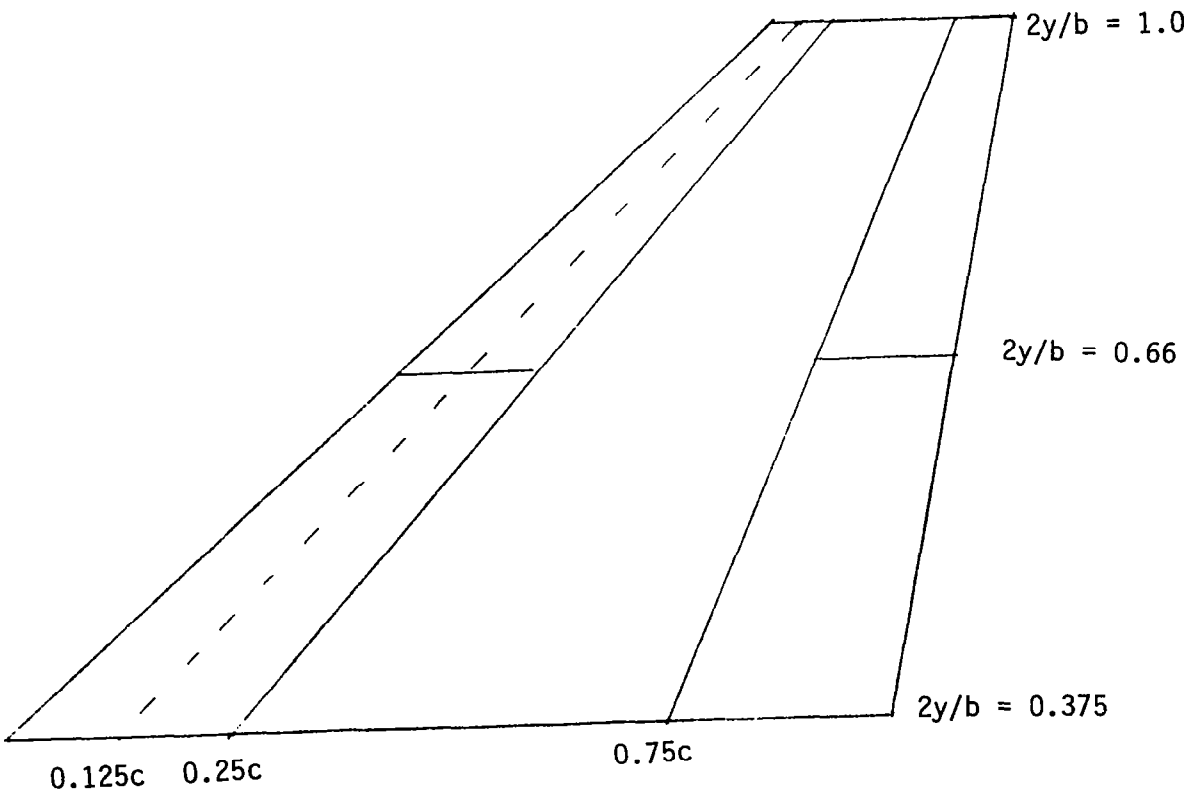

Candidate variable camber system deflections were derived by linear zero suction drag minimization using the finite element model of figure 20. The lift coefficient was constrained during the optimization. The angle of attack and deflection of the vertical tail, body flap and outboard wing panel leading and trailing edge devices are solved for at the various pertinent design conditions.

The foregoing discussion defines the salient considerations indicated as "linear initialization" on figure 16. The discussion of the nonlinear effort follows. Its basic intent is to achieve/verify pressure gradient management with the basic goal of controlling separation. As such, it addresses sufficient low drag considerations as opposed to linear necessary farfield requirements.

SUBSONIC

A full potential analysis[4] of the M = 0.5, C_L = 1.13 subsonic maneuver condition (α = 15 degrees) was conducted for a nominal tip twist of -7.5 degrees. The candidate variable camber system deflections derived from linear theory and peak leading edge suction pressure considerations are:

Device	2y/b	δ-deg
Leading edge	0.375 - 0.66	-15/-7.5
	0.66 - 1.0	-15/-7.5
Trailing edge	0.375 - 0.66	5
	0.66 - 1.0	5

The deflections are leading and trailing edge down to increase camber. Surface pressure and sectional loading results are presented in figure 21. The results based on a three dimensional boundary layer analysis[6] indicate the discrete hinge lines although apparent in the pressure distributions do not cause any particular problem. Separation is confined to aft of the trailing edge flap hinge line for the outboard 30 percent of the span for the nominal Rockwell test facility condition of $R_{N_{\bar{c}}} = 4.8 \times 10^6$.

TRANSONIC

Conservative small disturbance analysis[3] of the variable camber system was parametrically performed to define deflections required to control upper surface leading edge pressure peaks, increase shock sweep, and move the shock towards the trailing edge to maximize the extent of attached flow.

The resulting numerical flow quality for M = 0.9, C_L = 0.8 maneuver condition (α = 8 degrees) is presented in figure 22 for a nominal tip twist of -7.5 degrees. The deflections of the geared (two chordwise segment) leading edge and trailing edge variable camber system are:

Device	2y/b	δ-deg
Leading edge	0.375 - 0.66	-5.5/-2.75
	0.66 - 1.0	-5.5/-2.75
Trailing edge	0.375 - 0.66	2.5
	0.66 - 1.0	2.5

The deflections are leading and trailing edge down to increase the camber relative to the baseline (undeflected) condition. The spanwise variation of section lift is presented in figure 22c. A peak perpendicular value of 1.27 is being carried at 85 percent of the span. The nominal upper surface local shock Mach number is 1.4.

A transonic conservative full potential analysis[4] of the M = 0.9, C_L = 0.8 maneuver condition was subsequently performed to define the leading edge flow quality more accurately than the small disturbance theory was capable of since it uses chord plane transfer of boundary condition approximations. The angle of attack was increased from 8 to 9 degrees to match the small disturbance gross and outer panel local lift coefficent. The results are presented on figure 23 and indicate the discrete hinge lines, although apparent in the pressure distribution, do not cause any particular design problem. As a consequence, a smooth variable camber leading edge is not an aerodynamic performance requirement for the transonic maneuver design. The pressure peaks at the leading edge for the full potential result indicate a slightly larger deflection is required to achieve local ideal angle of attack conditions.

SUPERSONIC

Variable camber system design was performed at supersonic cruise and maneuver conditions. The development was initialized[2] using untrimmed zero suction drag due to lift optimization at M = 1.6, C_L = 0.1, and M = 1.6,

C_L = 0.32, respectively. The finite element model of figure 20 was used for this purpose. The resulting deflections are:

Condition	Device	2y/b	δ-deg
M = 1.6, C_L = 0.1	Leading edge	0.375 - 0.66	4.1/ 2.05
$\alpha = 1.24^o$		0.66 - 1.0	6.0/ 3.0
$\theta_t = 4.2^o$*			
	Trailing edge	0.375 - 0.66	-1.5
		0.66 - 1.0	-2.5
M = 1.6, C_L = 0.32	Leading edge	0.375 - 0.66	2.7/ 1.35
$\alpha = 5.22^o$		0.66 - 1.0	5.4/ 2.7
$\theta_t = -7.5^o$			
	Trailing edge	0.375 - 0.66	-0.9
		0.66 - 1.0	-1.7

The deflections in all cases are leading and trailing edge up as a result of the spar box camber (figure 19) incorporated for subsonic/transonic maneuver.

Supersonic full potential analysis[5] of these cases is presented on figure 24. The geometric model and typical grid used is presented on figures 24a and 24b, respectively. The flow over the inboard upper surface region ($\eta < 0.2$) is shocked at the beginning of the canopy and the sting housing of

*This value is an earlier status than that of figure 19.

the wind tunnel model as indicated by figures 24c and 24d. The former is a consequence of over the nose vision requirement. The latter is a testing support problem associated with the blended wing body arrangement under consideration. The outboard wing panel at cruise is shock free although the widely spaced underslung nacelles were not modeled during the design because of code limitations at the time. The outboard wing panel upper surface maneuver pressures are well behaved in the leading edge region and exhibit no cross-flow shocks. A swept compression region emanates from the forward inboard constrained region and terminates at the outboard trailing edge. Examination of the results indicate the tip region is operating below the ideal angle of attack as a result of the wing spar box compromise being considered and larger twist than optimum.

Finite difference boundary layer analyses[6] of both the cruise and maneuver cases indicate the flow outboard of 20 percent span is fully attached for the mean aerodynamic chord Reynolds number of 1.56×10^6 planned for the Langley Unitary Plan Wind Tunnel test.

Supersonic cruise and maneuver pretest assessment of the multipoint design is summarized on figure 25. Linear predictions indicate lift-drag ratio levels of 3.24 and 6.19, respectively, for the proposed Unitary Wind Tunnel test condition. Comparison with the point design result of figure 15 indicates a predicted 11.6 percent reduction results from multipoint compromises associated with wing sweep, airfoil leading edge radius, and twist and camber. Two-thirds of the penalty is associated with thickness considerations and one-third with drag due to lift. Full potential results indicate a 8.6 percent reduction in supersonic maneuver L/D.

TEST EVALUATION

The test apparatus and installation in the NASA Langley Unitary Plan Wind Tunnel[11] is presented on figure 26. Six component force flow measurements were conducted at the following nominal test conditions.

M_∞	P_t-lb/$_{ft^2}$	T_t-deg R	$R_{n_{\bar{c}}} \times 10^{-6}$
1.5	1051	584.7	1.56
1.6	1079		
1.8	1154		
2.0	1253		
2.5	1600	584.7	1.56

In addition, surface pressure, oil flow, and vapor screen data were taken at the design points.

Standard sting deflection and balance cavity corrections were applied to the angle of attack and drag coefficient respectively. Sand grain trips were used to fix transition at the fuselage nose, nacelle internal and external lips and wing/vertical tail leading edges to achieve a fully turbulent boundary layer condition for skin friction drag estimation.

Nacelle internal drag corrections[12] were applied when appropriate using

$$C_{D_i} = C_{F_i} \frac{Aw_i}{S} \cos(\alpha+\varepsilon)+2 \frac{S_c}{S} \frac{m}{m_\infty} \sin^2(\alpha+\varepsilon)$$

RESULTS

Lift, drag, and pitching moment results for the wing-body-vertical at M = 1.6 are presented in figure 27 for the 55-degree swept point design and figure 28 for the 48 degree swept multipoint design. The former corresponds to a 3.7 degree subsonic leading edge while the latter is a 3.3 degree supersonic edge.

Full potential predictions are in good agreement with test results of reference 12 and unpublished NASA data for both the point and multipoint design wings. Linear theory prediction of the lift for the point design wing at the design angle of attack of 4.46 degrees is 16 percent high. The discrepancy will have added significance when the levels of theoretical leading edge suction achieved are subsequently discussed.

A comparison of the point design measured and predicted aerodynamic efficiency is presented on figure 29. Equivalent flat plate full leading edge suction was projected for this case based on the design results of figure 9. Achievement of 60 percent theoretical suction levels is indicated based on flat plate linear theory prediction of lift curve slope. The 16 percent overprediction of lift of figure 27 is the apparent reason for this since adjustment of the zero suction flat plate result for differences in theoretical and experimental lift curve slope shifts the 100 percent suction result coincident with the measurements at the design condition. The conclusion here is that the indicated loss in leading edge suction is apparently due to nonlinear compressibility effects on lift.

Full potential nacelle on predictions are compared to measurement for the point design wing on figure 30. The associated surface grid is presented on figure 31. The predicted untrimmed maneuver lift-drag ratio is 6.6 percent optimistic and is considered to be in satisfactory agreement considering the uncertainties of internal drag correction. The full potential result compares to 8.9 percent optimistic linear theory prediction. Lift at the design angle of attack is somewhat over predicted. The pitching moment is pessimistic and not as good as the nacelle off result of figure 27.

Oil flow photographs indicate the existence of a normal shock ahead of the model pitot type inlet. The associated high surface pressure region and associated local separation is consistent with higher drag and more positive pitching moment coefficient (since the area is located ahead of reference point) than predictions which neglect such effects.

The full configuration supersonic full potential analysis of figure 30 required 480 cpu seconds on the Rockwell CYBER 875 serial computer under OPT=2 compilation. Subsequent restructuring and execution on the Rockwell CRAY X-MP/14 parallel processor reduced this time to 35 seconds.

Finally, an evaluation of the impact of multipoint compromise associated with decreases in planform sweep and increase in section leading edge radius, camber, and twist is presented on figure 32. A decrease in untrimmed maneuver design L/D of 7.0 percent results and compares to 8.6 percent for the nacelle off case. Predictions overstate the full configuration absolute efficiency in both cases and the effect of the compromise.

A 55-degree leading edge sweep flat reference panel was also tested in the present study to provide an assessment of the benefit of twist and camber for the point design wing. Its aerodynamic efficiency was essentially the same for a range of test Mach number and lift. This is apparently a result of rigging the reference wing at -1.5 degree incidence in order to attach it to the inboard blended wing body. It has been previously found[13] that operating a wing in the upwash field of a body allows it to generate a fixed lift at a lower angle of attack and consequently reduces the drag due to lift $C_L \tan \alpha$. This design approach consequently is an alternate to the one considered here. Clearly it requires a different aerodynamic philosophy at subsonic/transonic conditions where variable camber was used to control and reduce separation at higher lift.

CONCLUSIONS

Based on the numerical development and supersonic test results described in this document, the following conclusions are made.

1. An efficient supersonic nonlinear point design wing panel was numerically developed and test validated.

2. An efficient nonlinear multipoint wing design was developed for trisonic maneuver and supersonic cruise. Its goal of high subsonic/transonic aerodynamic efficiency without significantly penalizing supersonic performance was validated by Rockwell tests.

3. Supersonic test evaluation indicates the differences between multipoint and point design aerodynamic maneuver efficiency are modest.

4. Comparison between supersonic full potential prediction and experimental results for a representative advanced tactical fighter arrangement were good.

5. Linear theory provided a satisfactory initialization procedure for the present nonlinear design effort.

REFERENCES

1. Bonner, E.; Clever W.; and Dunn, K.: "Aerodynamic Preliminary Analysis System II - Part I, Theory" NASA CR-165627, April 1981.

2. Clever, W. C.: "Supersonic Second Order Analysis and Optimization Program User's Manual," NASA CR-172342, September 1984.

3. Mason, W. H.; et. al.: "An Automated Procedure for Computing the Three-Dimensional Transonic Flow Over Wing-Body Combinations, Including Viscous Effects," Volume I - Description of Analysis Methods and Application, AFFDL-TR-77-122, February 1978. (Available from DTIC as AD A055 899.)

4. Caughey, D. A.; and Jameson, A.: "Recent Progress in Finite Volume Calculations for Wing-Fuselage Combinations," AIAA Paper 79-1513, July 1979.

5. Shankar, V.; and Szema, K. Y.: "Nonlinear Potential Analysis Techniques for Supersonic Aerodynamic Design," NASA CR-172507, March 1985.

6. Nash, J.; and Scruggs, R.: "An Automated Procedure for Computing the Three-Dimensional Transonic Flow Over Wing-Body Combinations, Including Viscous Effects," Volume III - An Implicit Method for the Calculation of Three Dimensional Boundary Layers on Finite, Thick Wings. AFFDL-TR-77-122, February 1978. (Available from DTIC as AD A055 263.)

7. Gingrich, P.B.; Child, R. D.; and Panageas, G. N.: "Aerodynamic Development of the Highly Maneuverable Aircraft Technology Remotely Piloted Research Vehicle," NASA CR-143841, June 1977.

8. Bonner, E.; and Gingrich, P. B.: "Transonic Computational Experience for Advanced Tactical Aircraft," Progress in Astronautics and Aeronautics Vol. 81 Transonic Aerodynamics, D. Nixon Editor, American Institute of Aeronautics and Astronautics, 1982.

9. Gingrich, P. B.; and Bonner, E.: "Wing Design for Supersonic Cruise/ Transonic Maneuver Aircraft," 13th Council of the International Council of Aeronautical Sciences, Vol. 2, American Institute of Astronautics, August 1982.

10. Bonner, E; and Gingrich, P. B.: "Supersonic Cruise/Transonic Maneuver Wing Section Development," Air Force Flight Dynamics Laboratory Report AFAWL-TR-80-3047, June 1980.

11. Jackson, C. M., Jr.; Corlett, W. A.; and Monta, W. J.: "Description and Calibration of the Langley Unitary Plan Wind Tunnel," NASA TP-1905, November 1981.

12. Shrout, B. L.; and Talcott, N. A., Jr.: "Effects of Wing Sweep and Camber on the Aerodynamic Characteristics of a Fighter Configuration at Supersonic Speeds," NASA TM-86427, 1985.

13. Shrout, B. L.; and Robins, A. W.: "Longitudinal Aerodynamic Characteristics of an Elliptical Body with a Horizontal Tail at Mach Numbers From 2.3 to 4.63," NASA TP-2024, June 1982

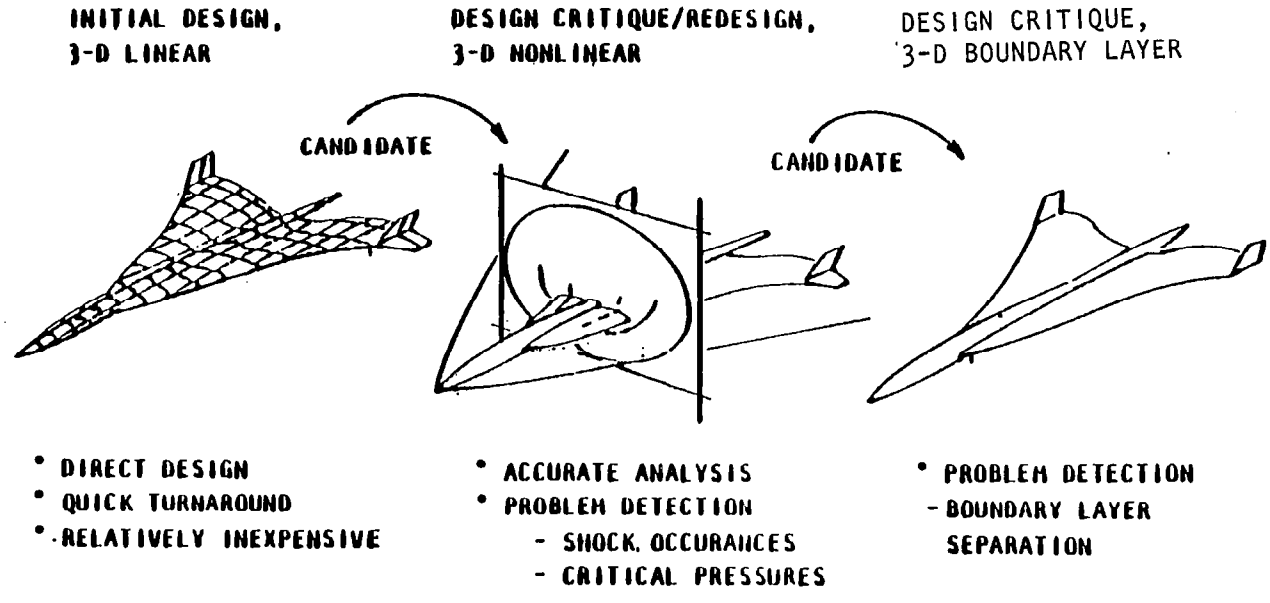

Figure 1. Numerical Design Approach

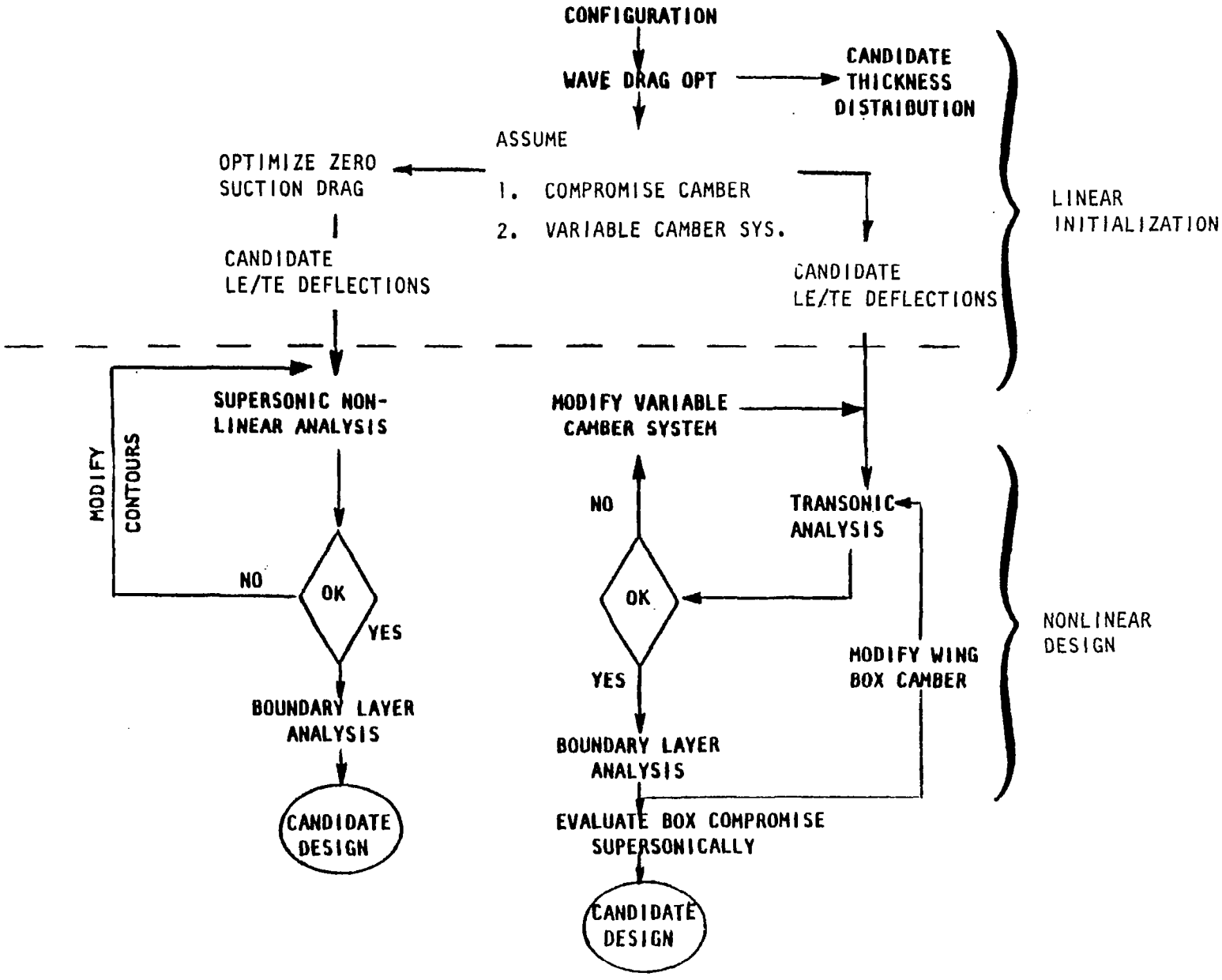

Figure 2. Example Design Cycle

METHOD	CAPABILITY AND FUNCTION	APPROXIMATIONS
INVISCID LINEAR POTENTIAL THEORY:		
DISTRIBUTED PANEL	SUBSONIC/SUPERSONIC MULTIPLE SURFACE DESIGN AND ANALYSIS WITH BODY	CHORD PLANE SINGULARITIES
SUPERSONIC AREA RULE	VOLUME OPTIMIZATION FOR MINIMUM WAVE DRAG	SLENDER-BODY
INVISCID NONLINEAR POTENTIAL THEORY:		
SMALL DISTURBANCE	TRANSONIC WING-BODY DESIGN AND ANALYSIS	BOUNDARY CONDITION TRANSFER
	SUPERSONIC WING-BODY OPTIMIZATION AND ANALYSIS	SECOND ORDER
FULL POTENTIAL	TRANSONIC WING-BODY ANALYSIS, EXACT BOUNDARY CONDITION	POTENTIAL FLOW
	SUPERSONIC WING-BODY ANALYSIS EXACT BOUNDARY CONDITIONS	POTENTIAL FLOW
VISCOUS ANALYSIS:		
3-D BOUNDARY LAYER	WING-LAMINAR/TURBULENT FINITE DIFFERENCE SOLUTION	YAWED WING EDGE APPROXIMATIONS, NO INTERACTION

Figure 3. Numerical Methodology

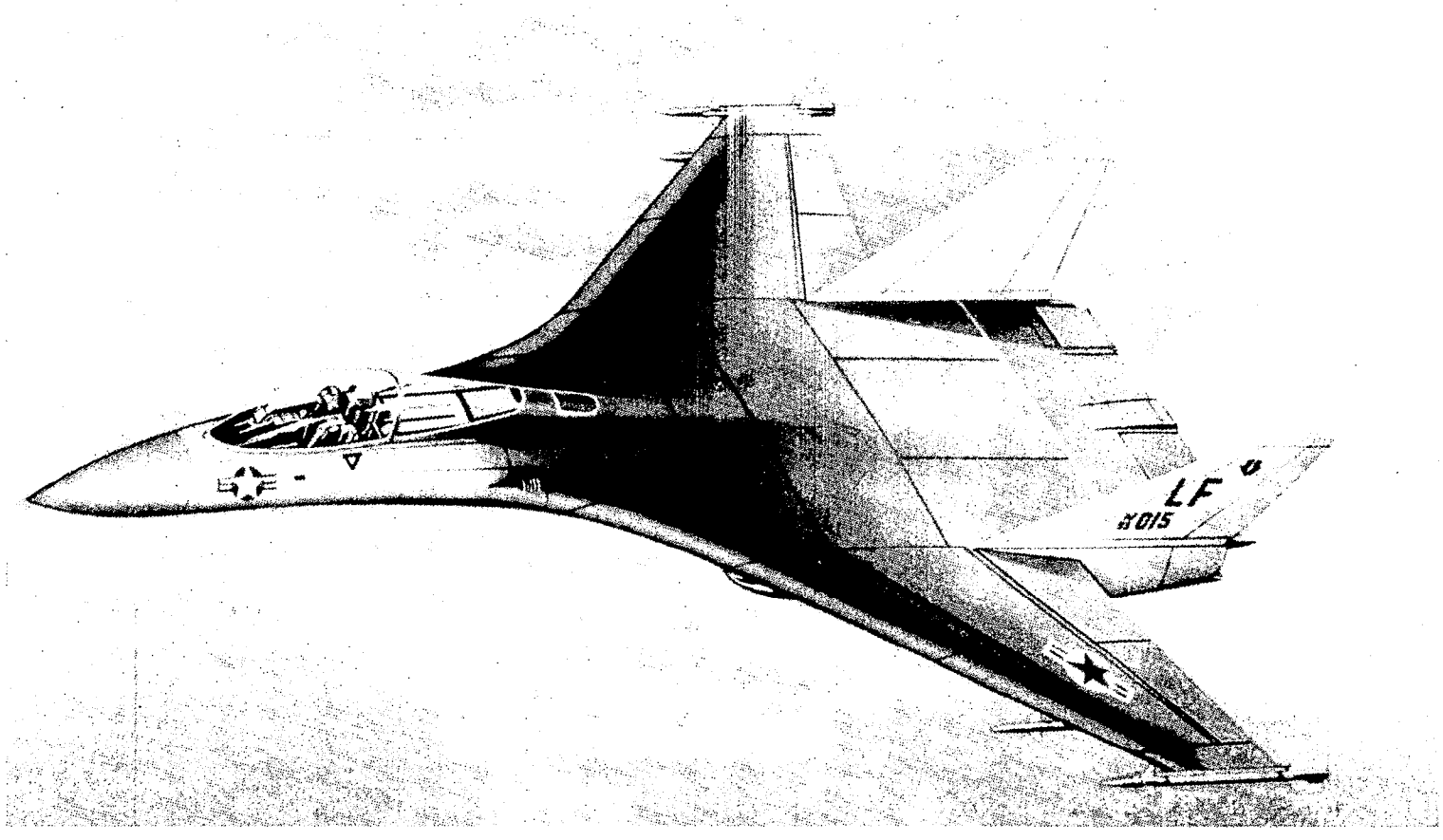

a) Isometric

Figure 4. Advanced Tactical Fighter Concept

GEOMETRIC PARAMETER	WING (TRAP)	VERTICAL (TRAP)
ASPECT RATIO	3	1
TAPER RATIO	0.2	0.2
LE SWEEP	48°	55°
DIHEDRAL	0	70°
THICKNESS RATIO	0.04	0.04

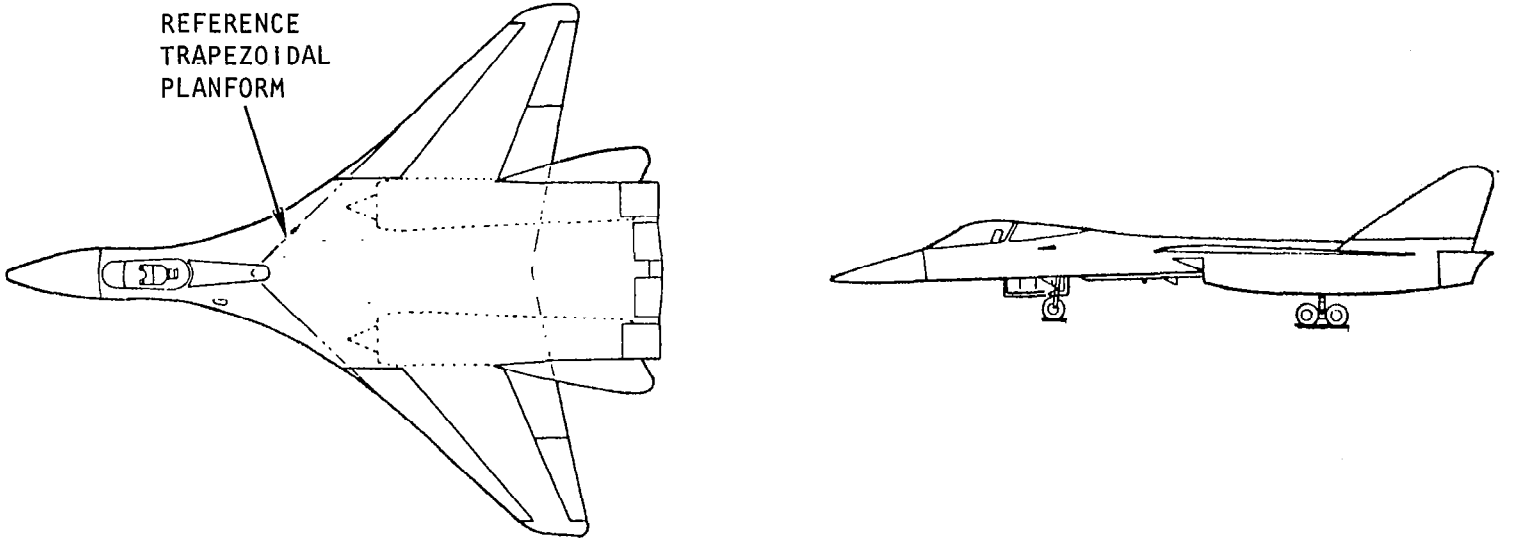

b) TWO VIEW

Figure 4. Concluded

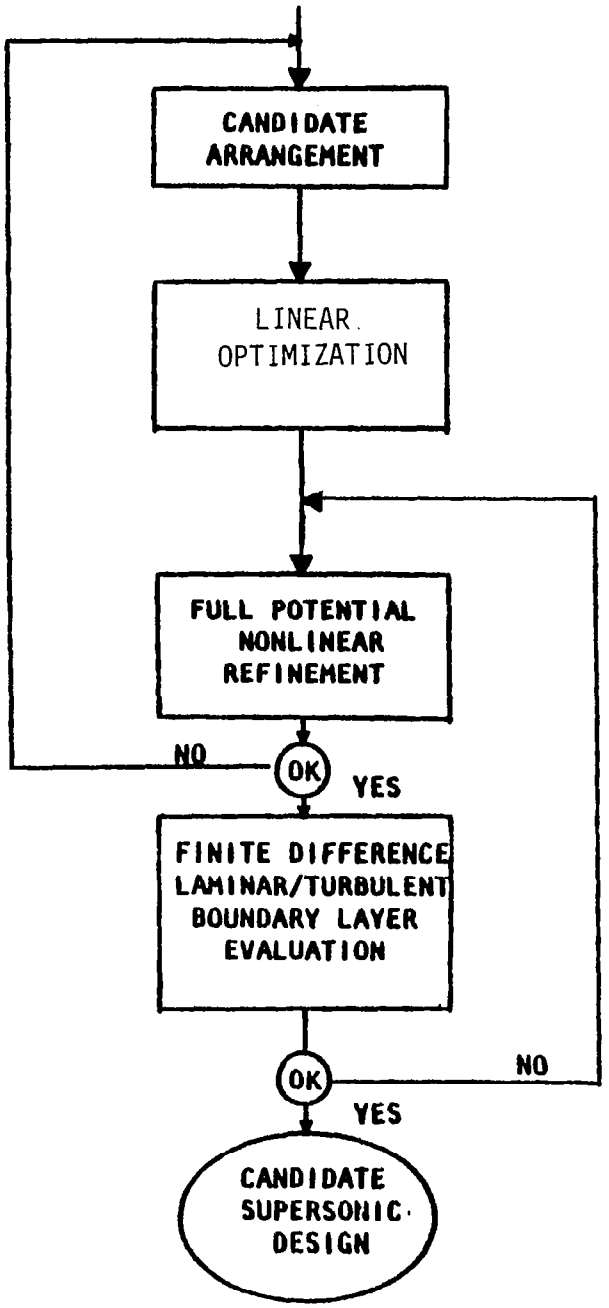

Figure 5. Supersonic Point Design Cycle

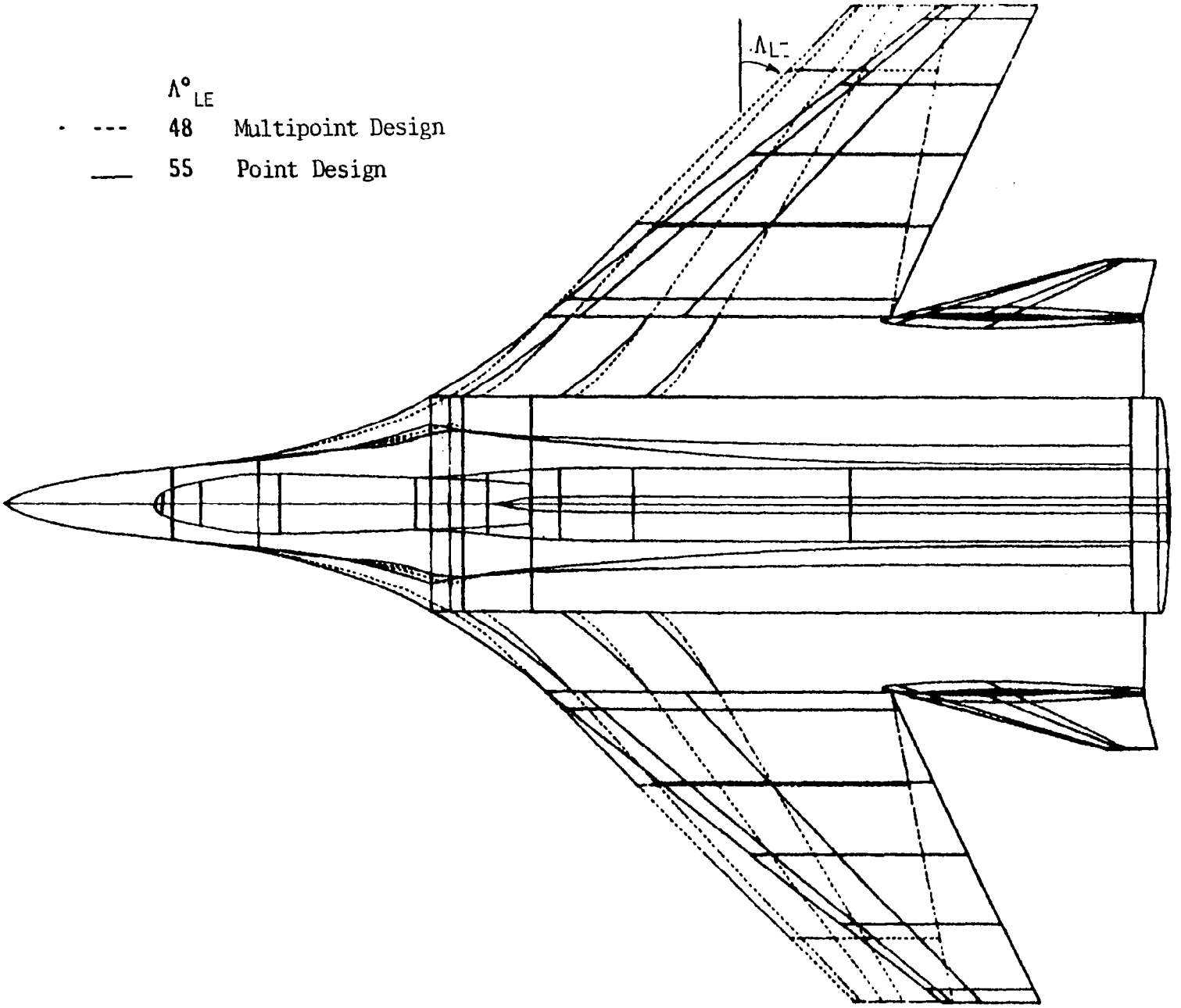

Figure 6. General Arrangement

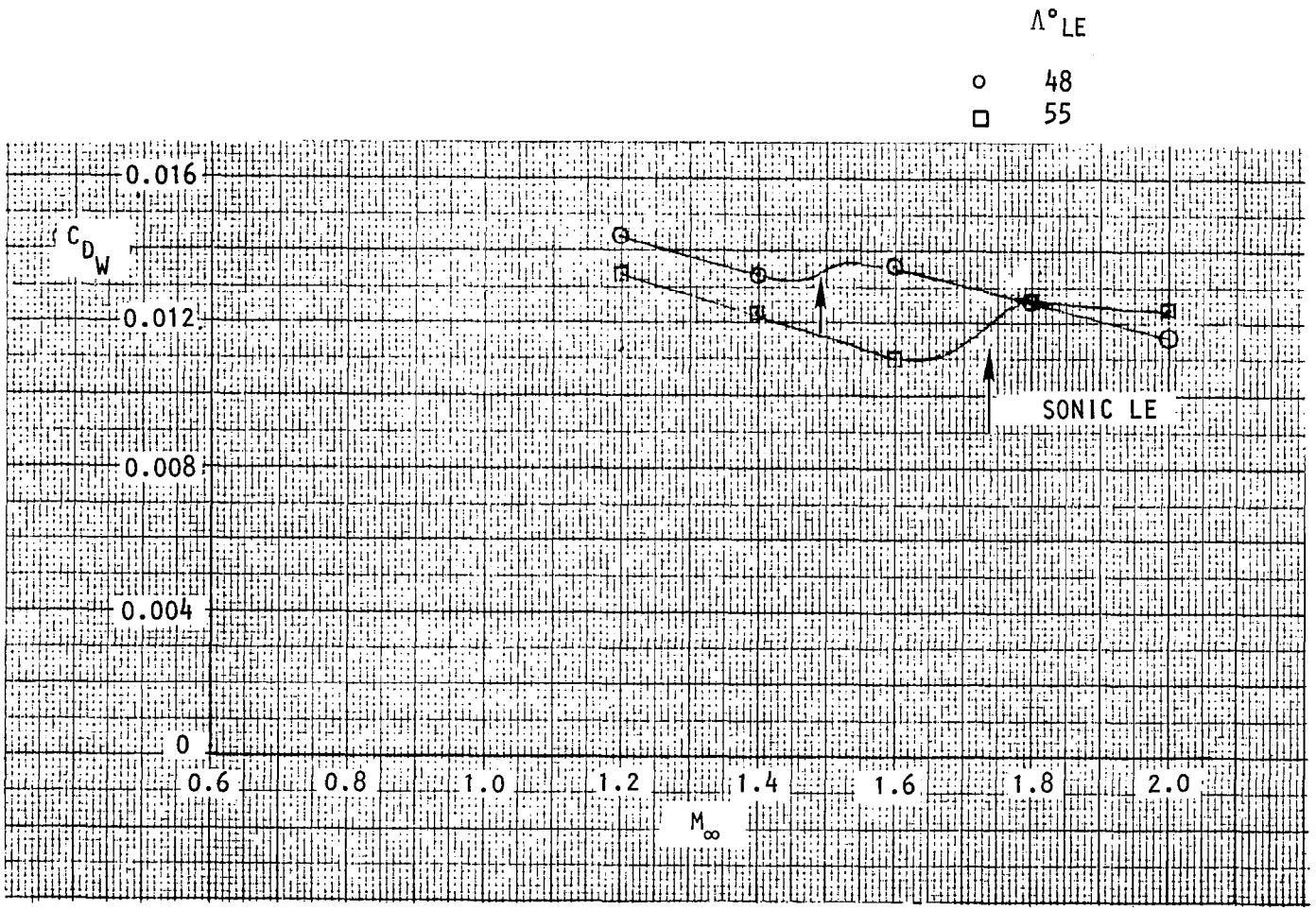

Figure 7. Effect of Sweep on Wave Drag

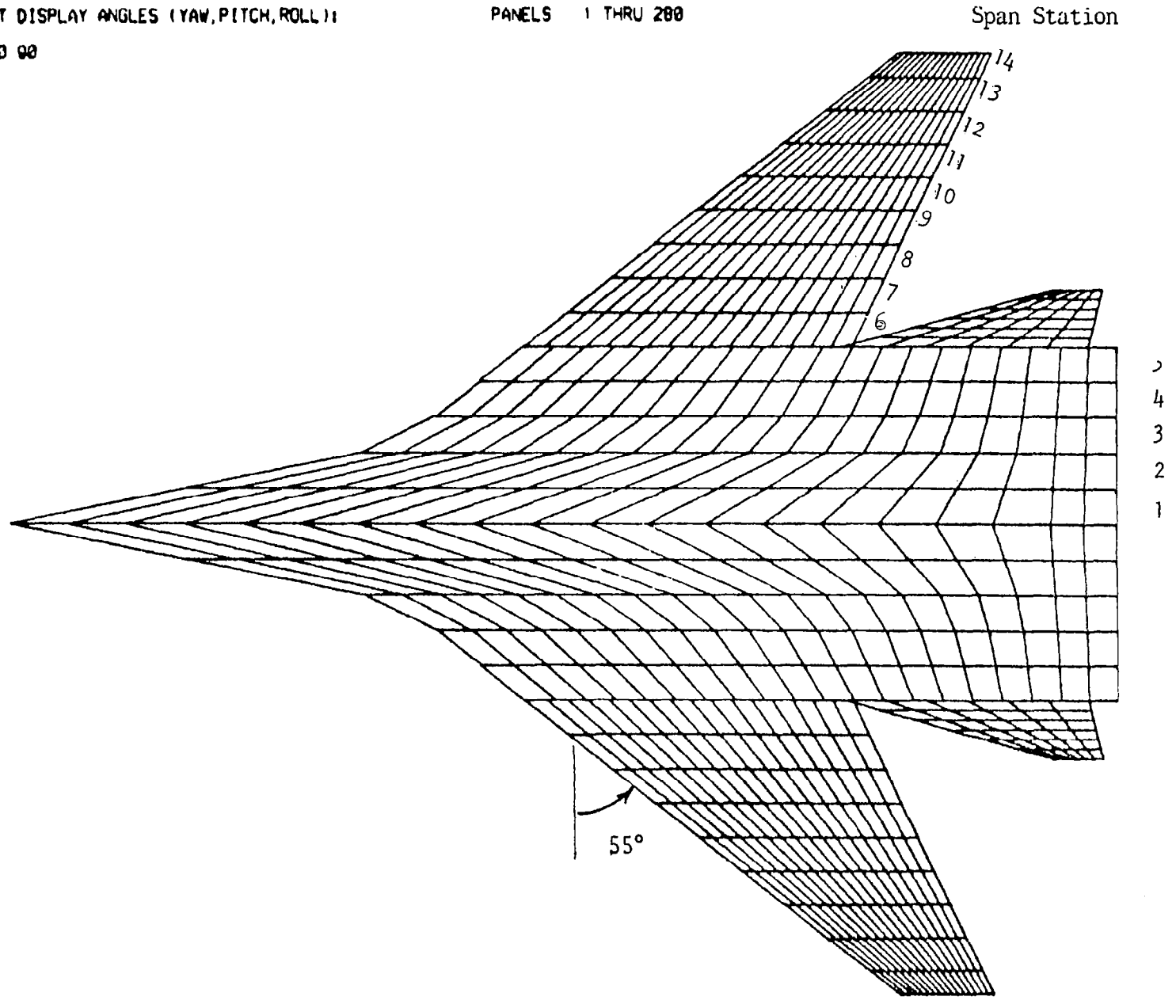

Figure 8. Linear Theory Finite Element Model

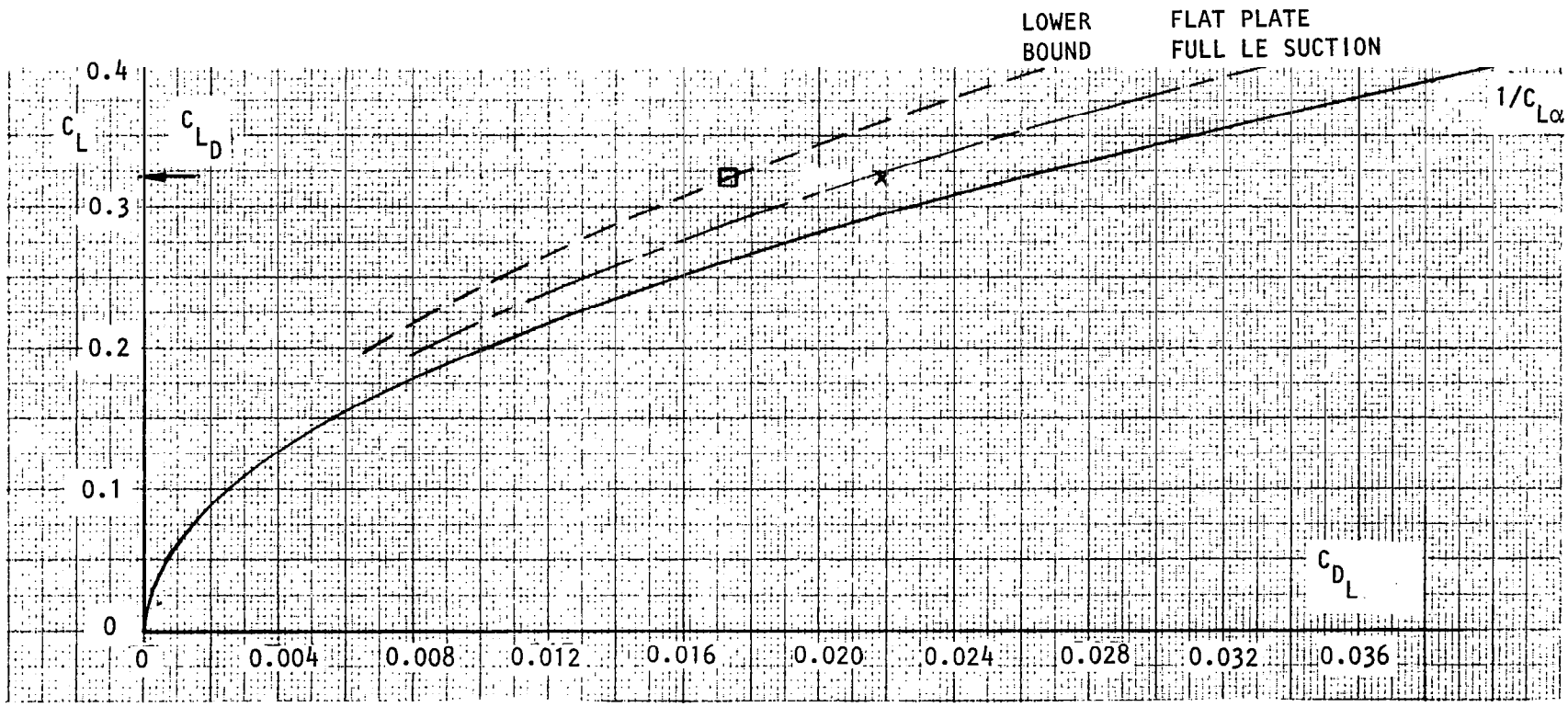

Figure 9. Zero Suction Drag Due to Lift Optimization at M = 1.6

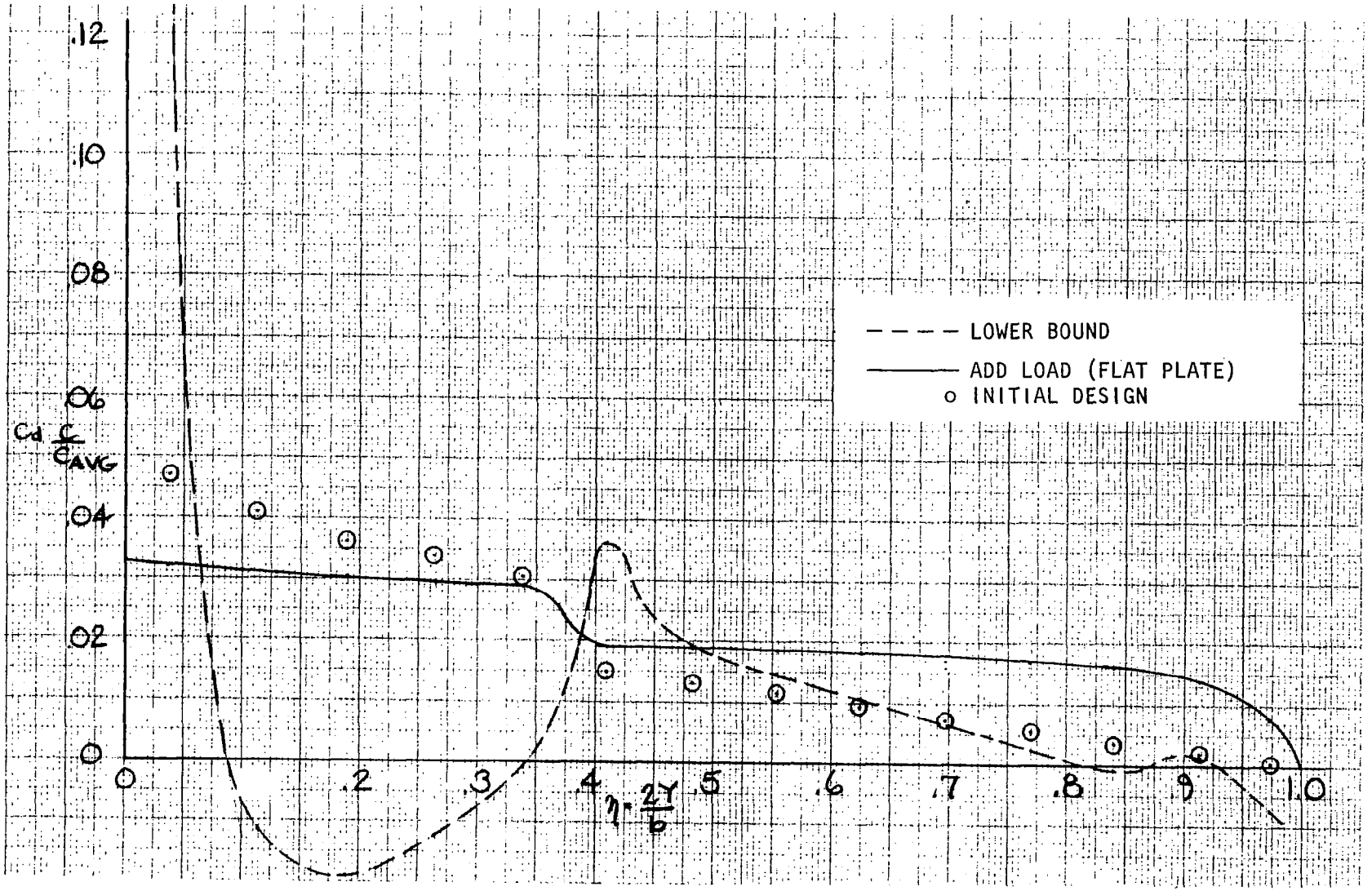

Figure 10. Spanwise Variation of Zero Suction Drag at M = 1.6, C_L = 0.32

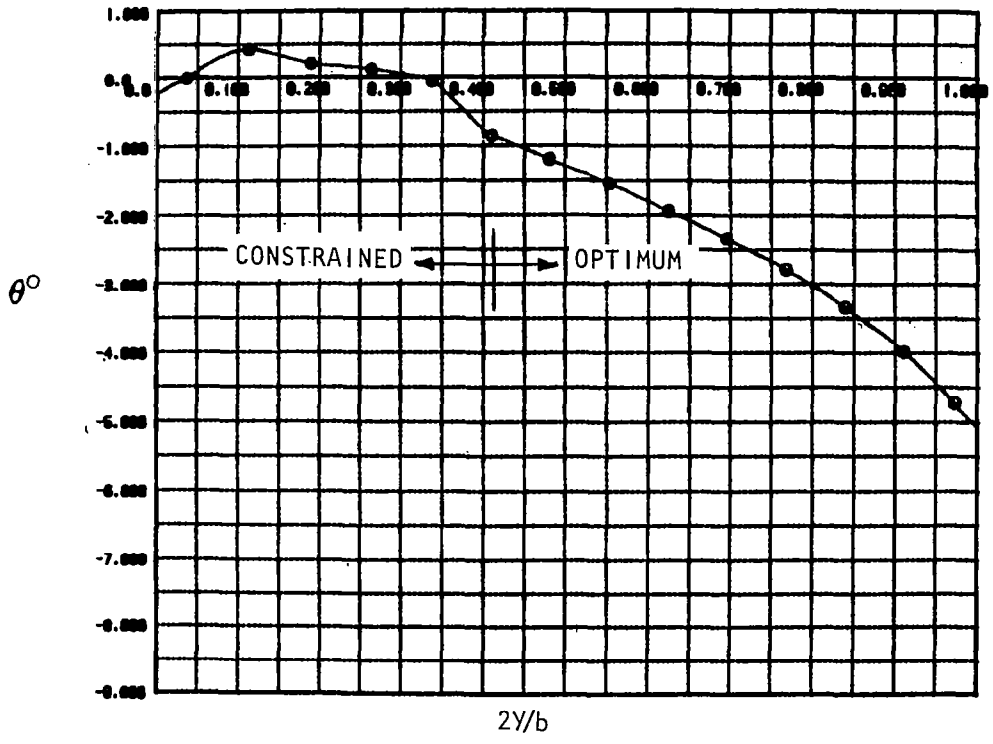

a) TWIST

Figure 11. Point Design Candidate Twist and Camber
M = 1.6, C_L = 0.32

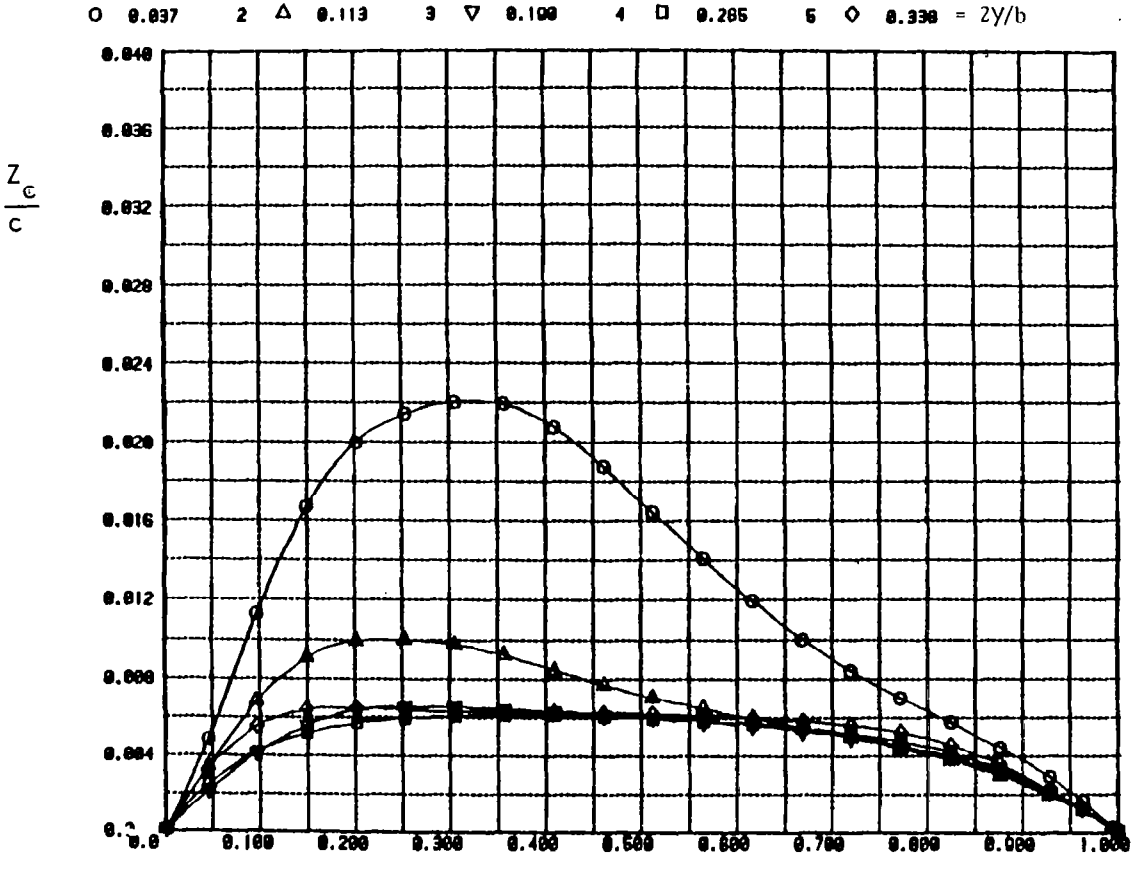

b) CONSTRAINED INBOARD CAMBER

Figure 11. Continued

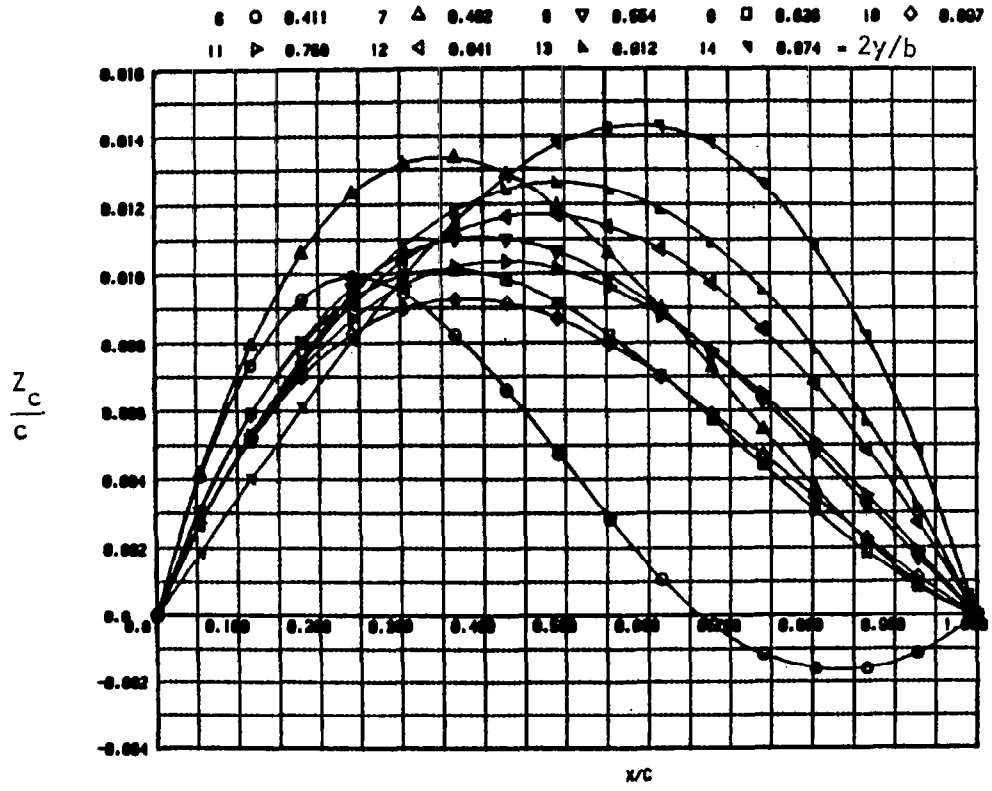

c) OPTIMUM OUTBOARD CAMBER

Figure 11. Concluded

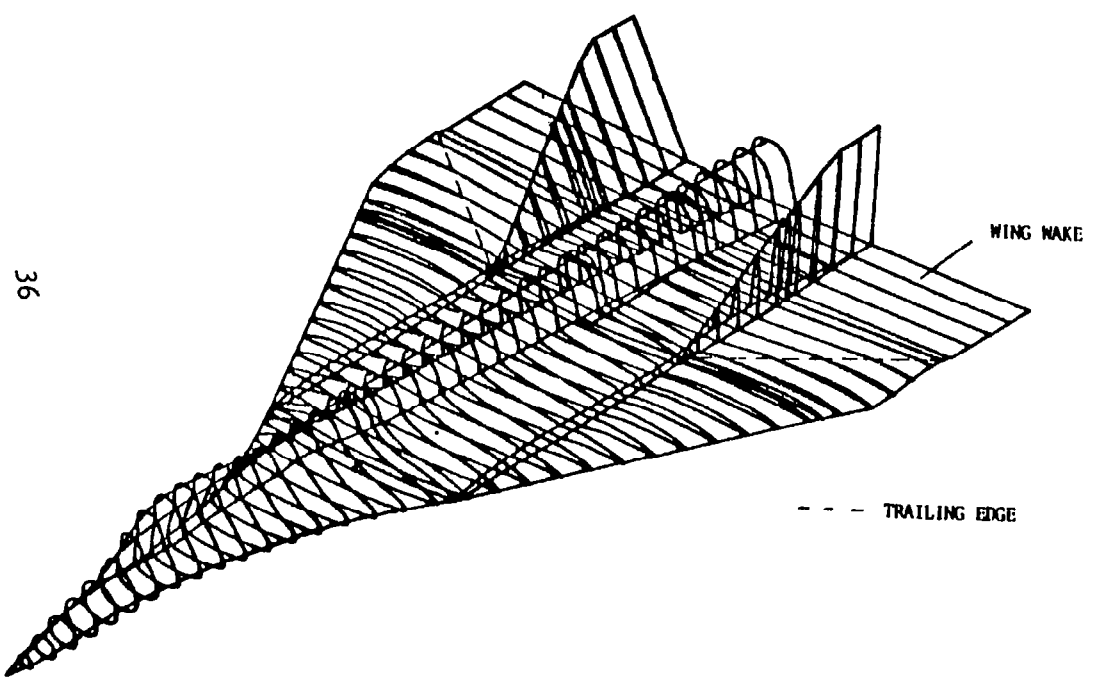

a) Geometric Model

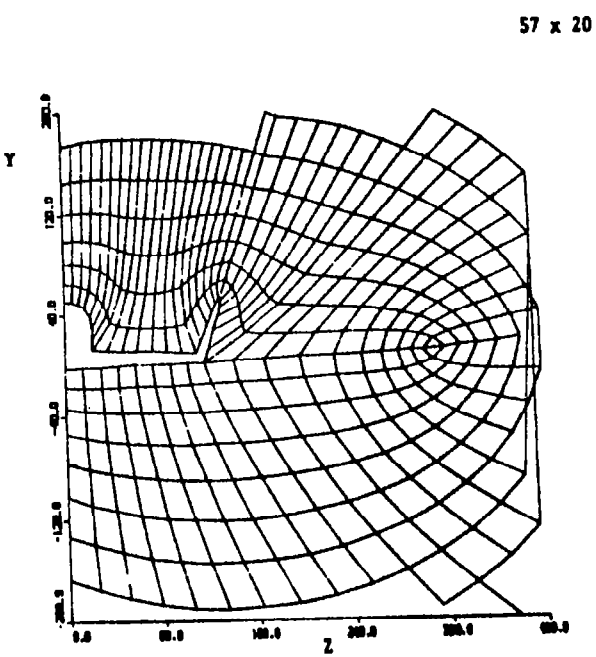

b) Body-Vertical Tail-Wing Wake Grid

Figure 12. Supersonic Maneuver Full Potential Analysis

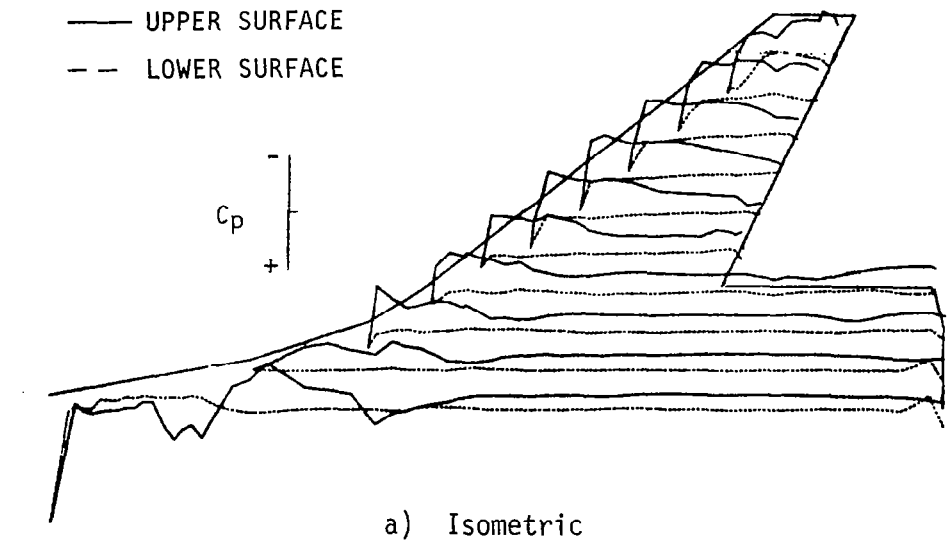

a) Isometric

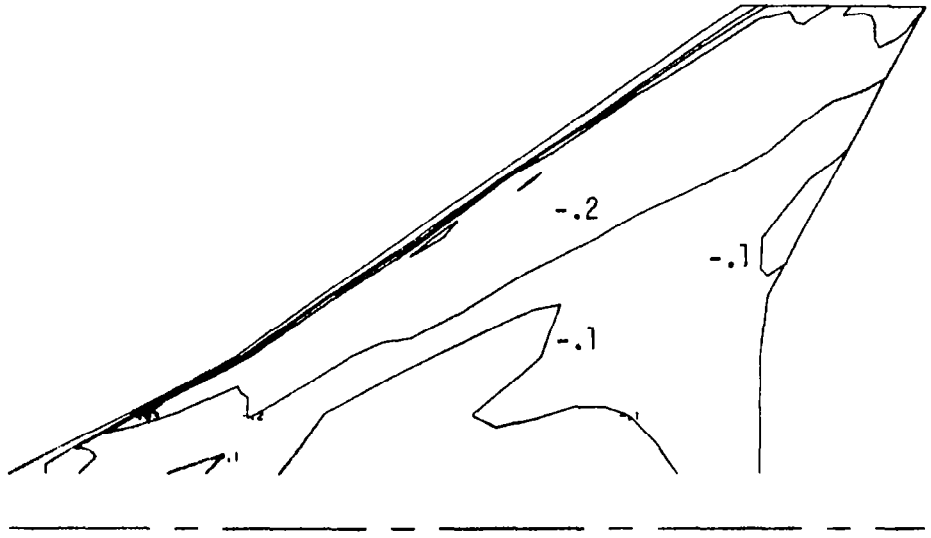

b) Upper Surface Isobars

Figure 13. Supersonic Maneuver Full Potential Surface Pressure Results
M = 1.6, C_L = 0.32, α = 4.46 Degrees

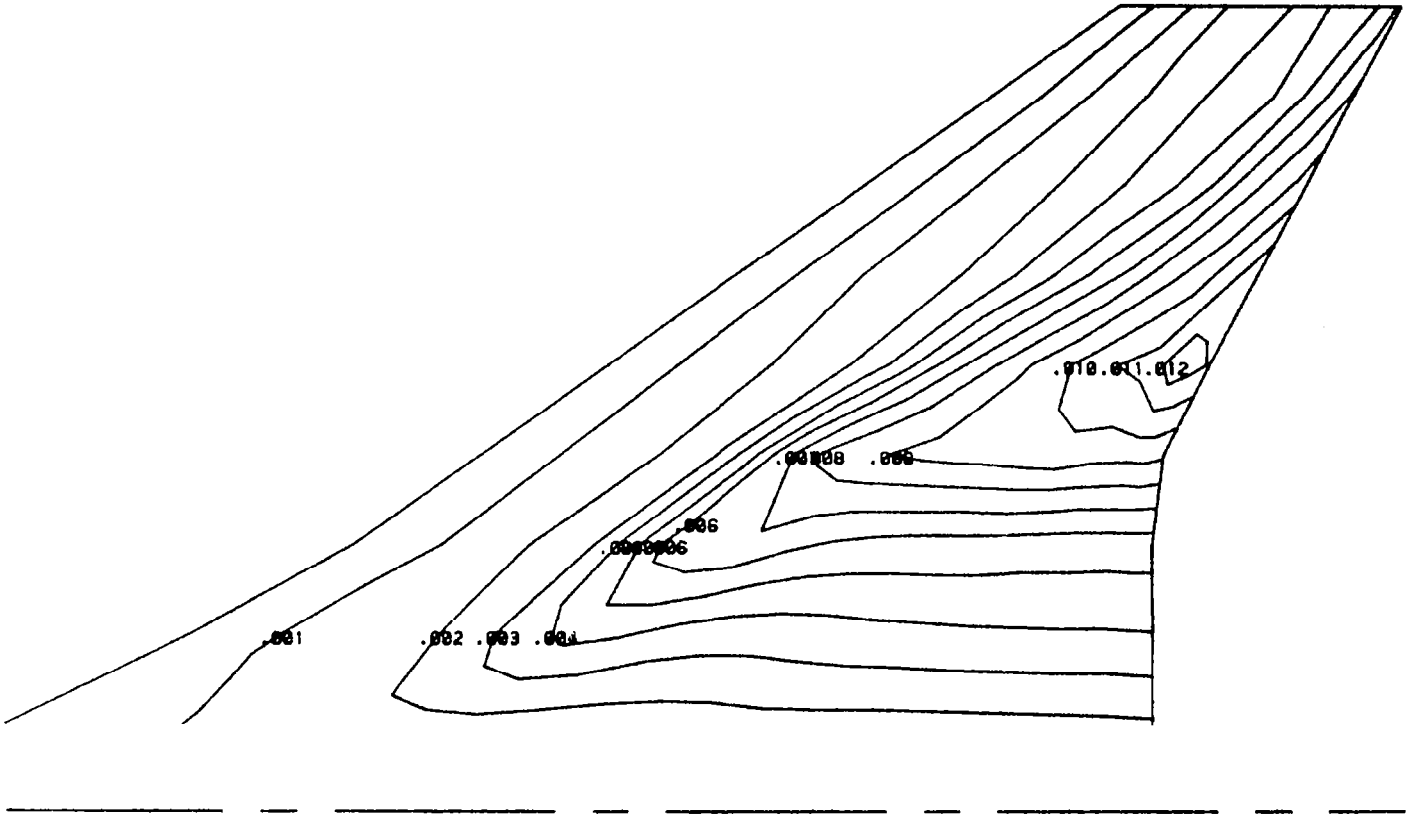

a) DISPLACEMENT THICKNESS, δ^*/C

Figure 14. Supersonic Maneuver Upper Surface Boundary Layer Analysis
$M = 1.6$, $C_L = 0.3$, $R_{N_{\bar{C}}} = 1.56 \times 10^6$

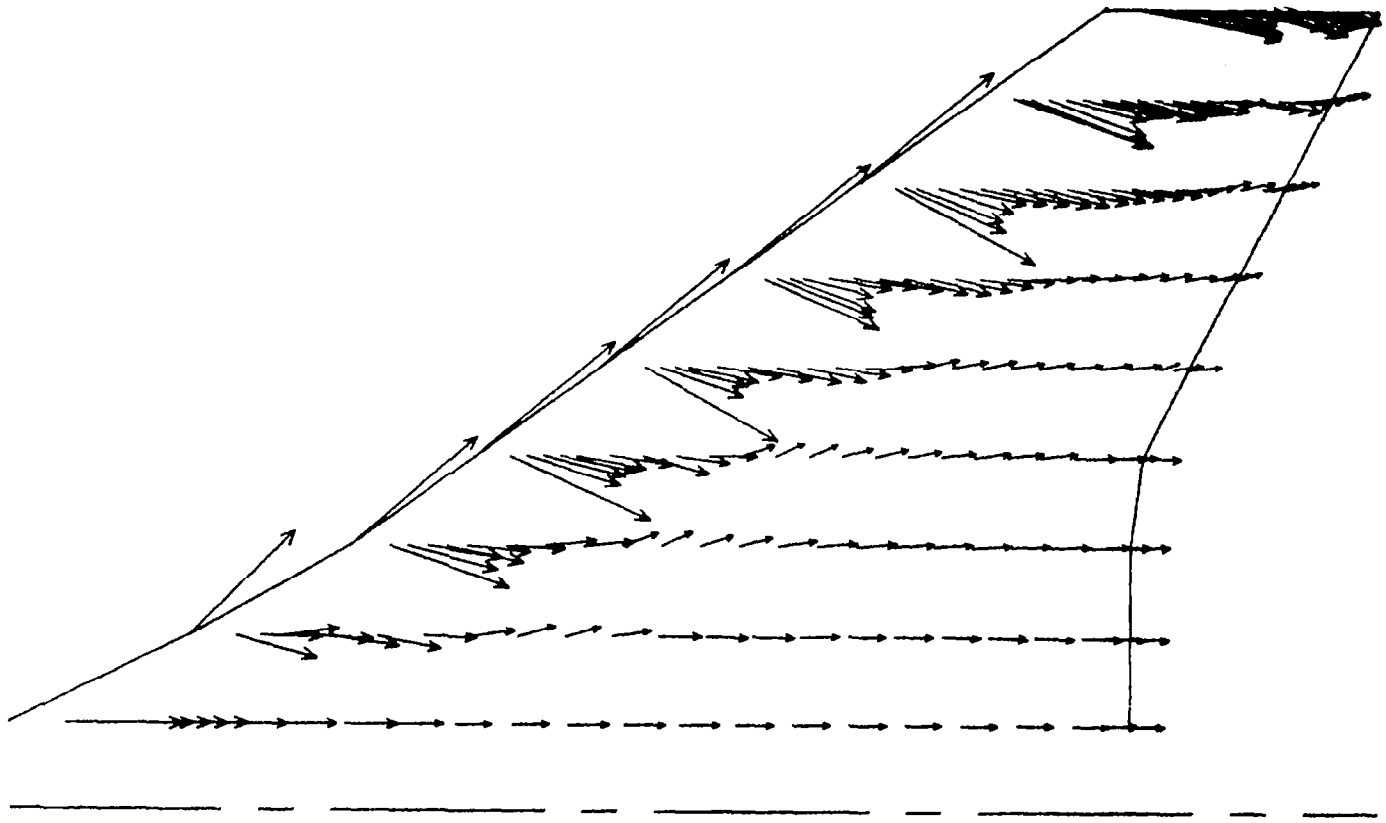

b) WALL SHEAR STRESS VECTORS

Figure 14. Concluded

Turbulent Skin Friction

C_{D_F} = 0.0129 at nominal test conditions, $R_{N_{\bar{c}}} = 1.56 \times 10^6$

Linear Analysis

α = 4.46 deg

C_L = 0.32

$C_{D_p} = C_{D_w} + C_{D_L}{}^* = 0.109 + 0.02185 = 0.03275$

C_M = -0.061

L/D = 0.32/(0.0129 + 0.03275) = 7.0

Full Potential

α = 4.46 deg

C_L = 0.311

C_{D_p} = 0.0325

C_M = -0.0579

L/D = 0.311/(0.0129 + 0.0325) = 6.85

*Cambered plate fuselage

Figure 15. Pretest M = 1.6 Maneuver 55-Degree Point Design Drag Assessment, Nacelle On

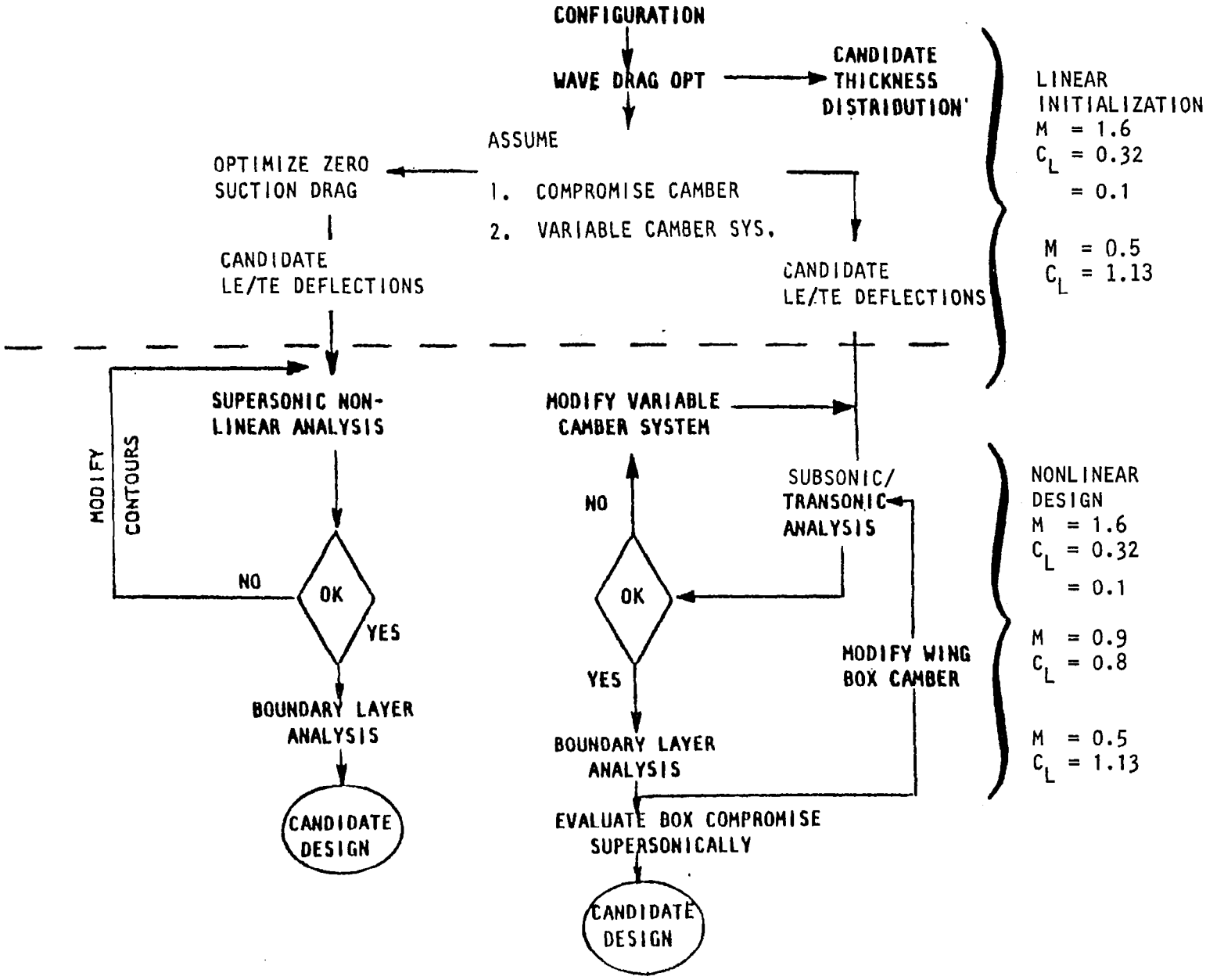

Figure 16. Multipoint Design Cycle

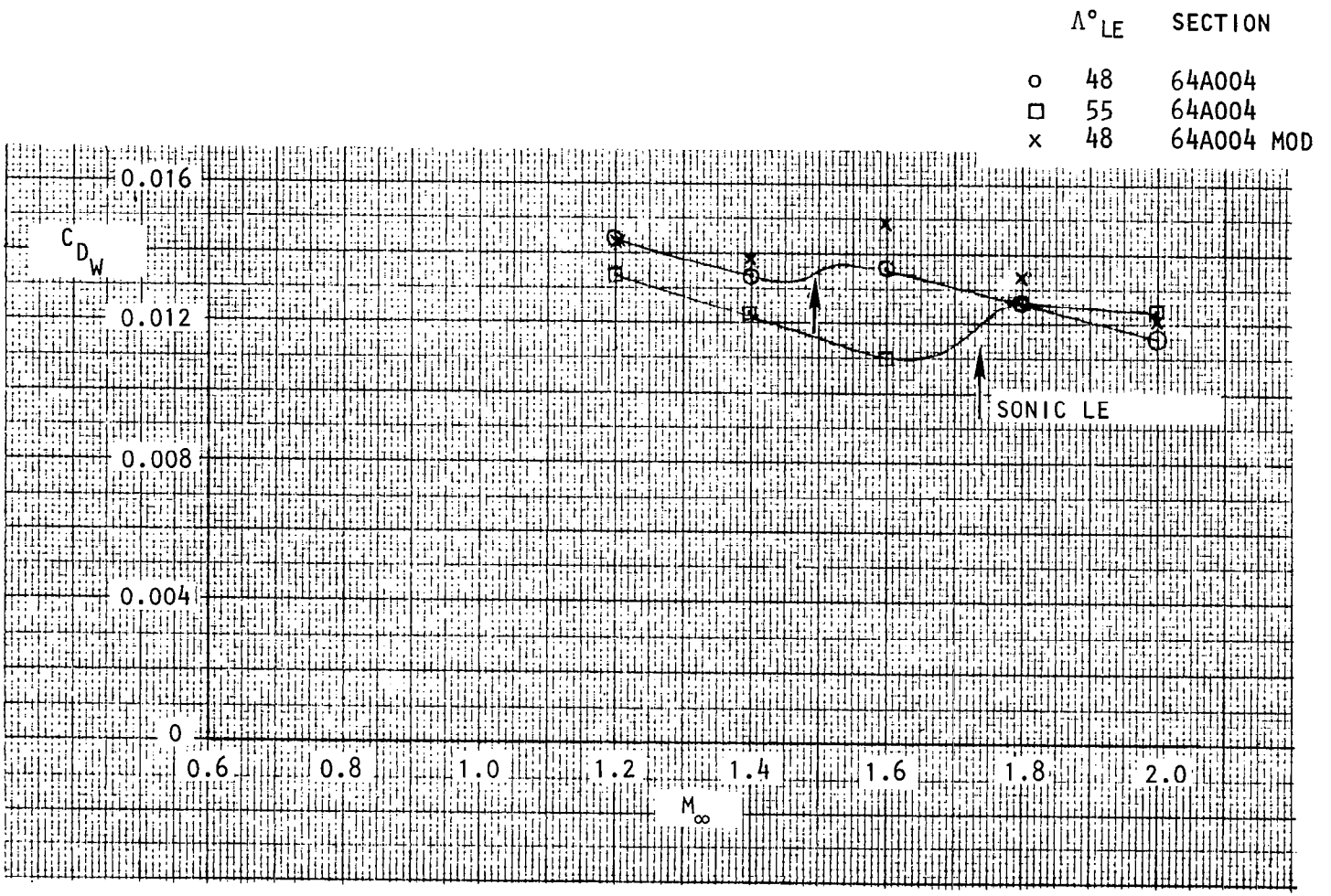

Figure 17. Effect of Multipoint Compromises on Wave Drag

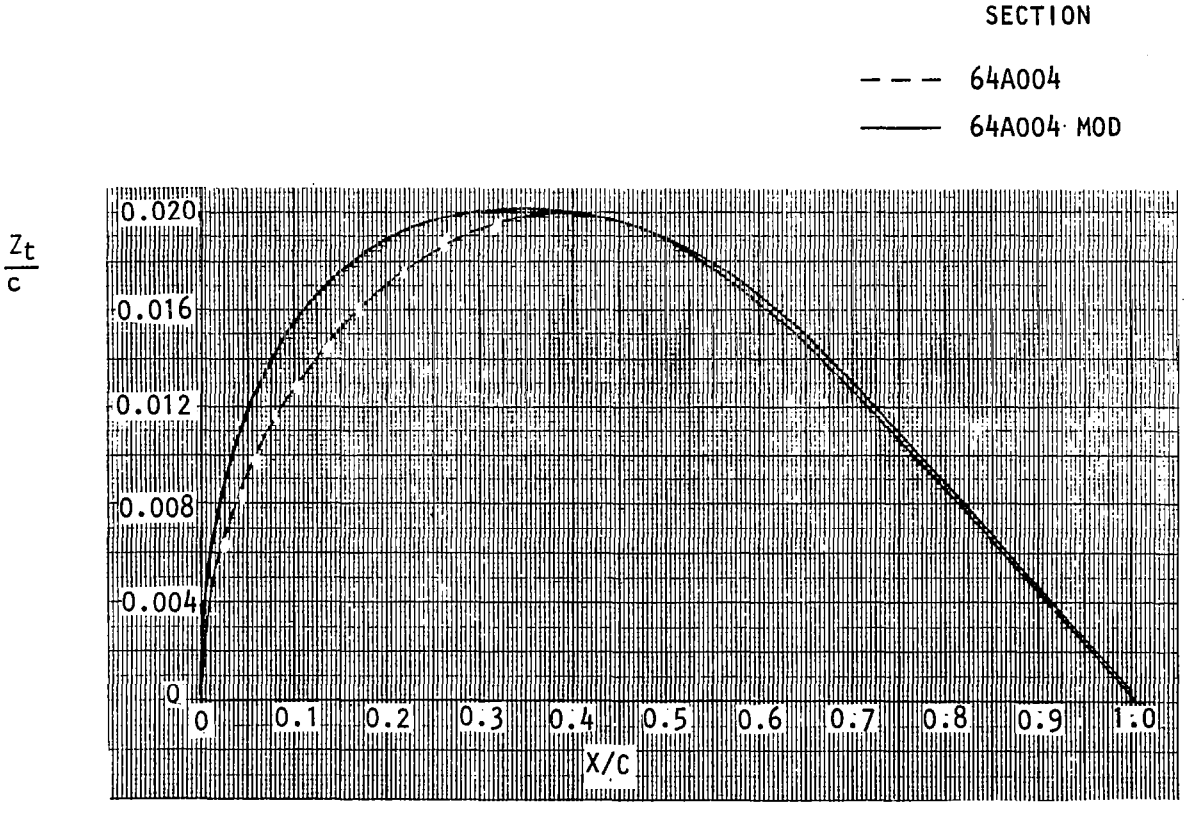

Figure 18. Outboard Panel Thickness Distribution

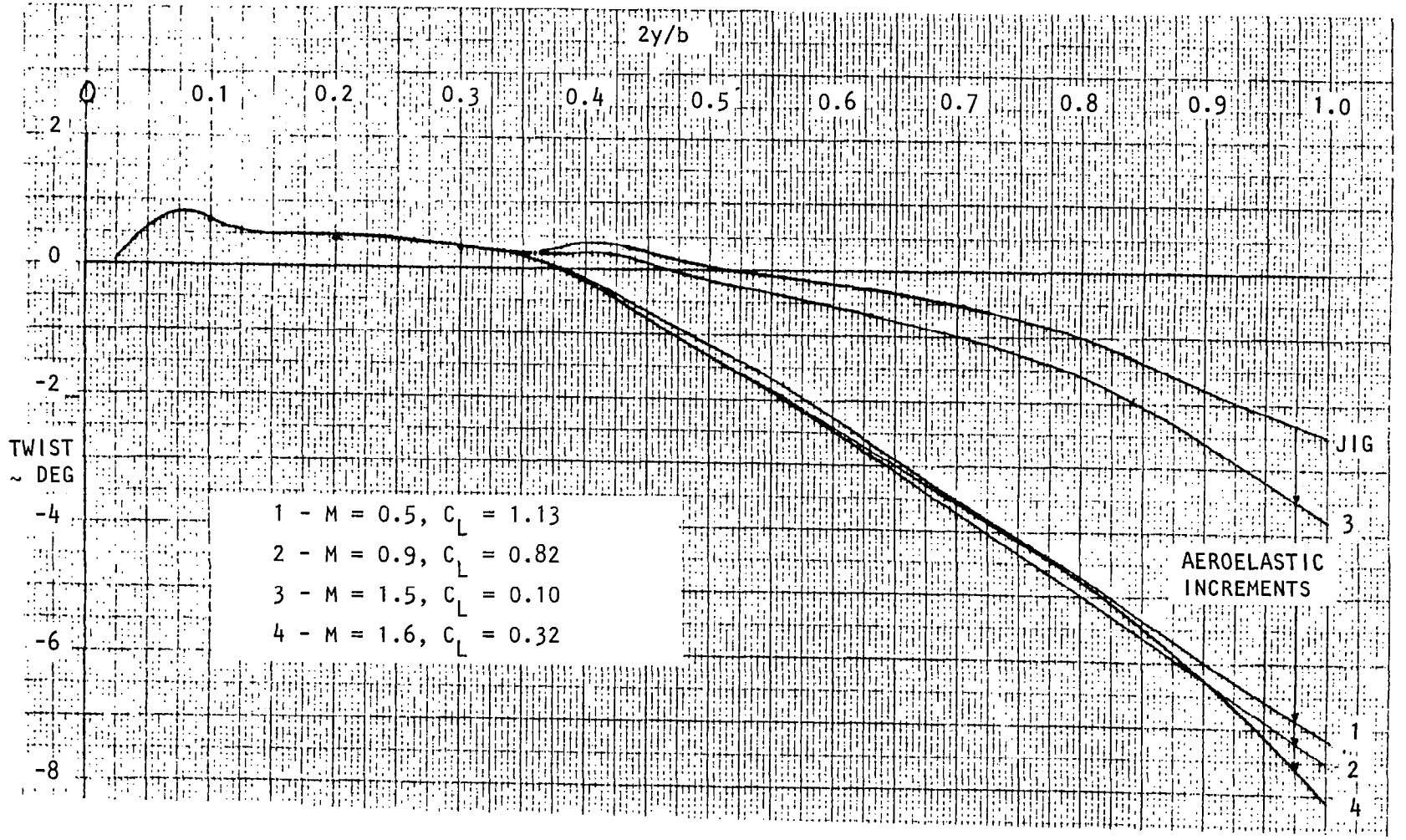

a) TWIST

Figure 19. Multipoint Design Candidate Twist and Camber

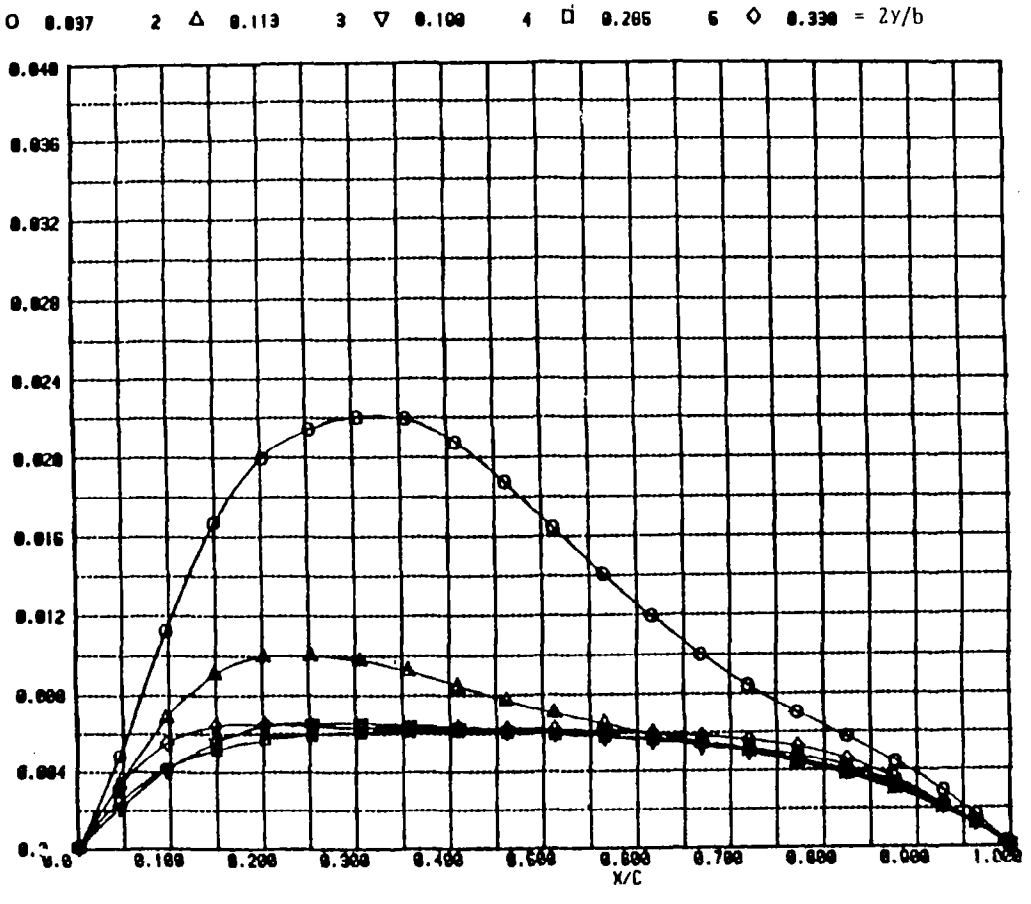

b) CONSTRAINED INBOARD CAMBER

Figure 19. Continued

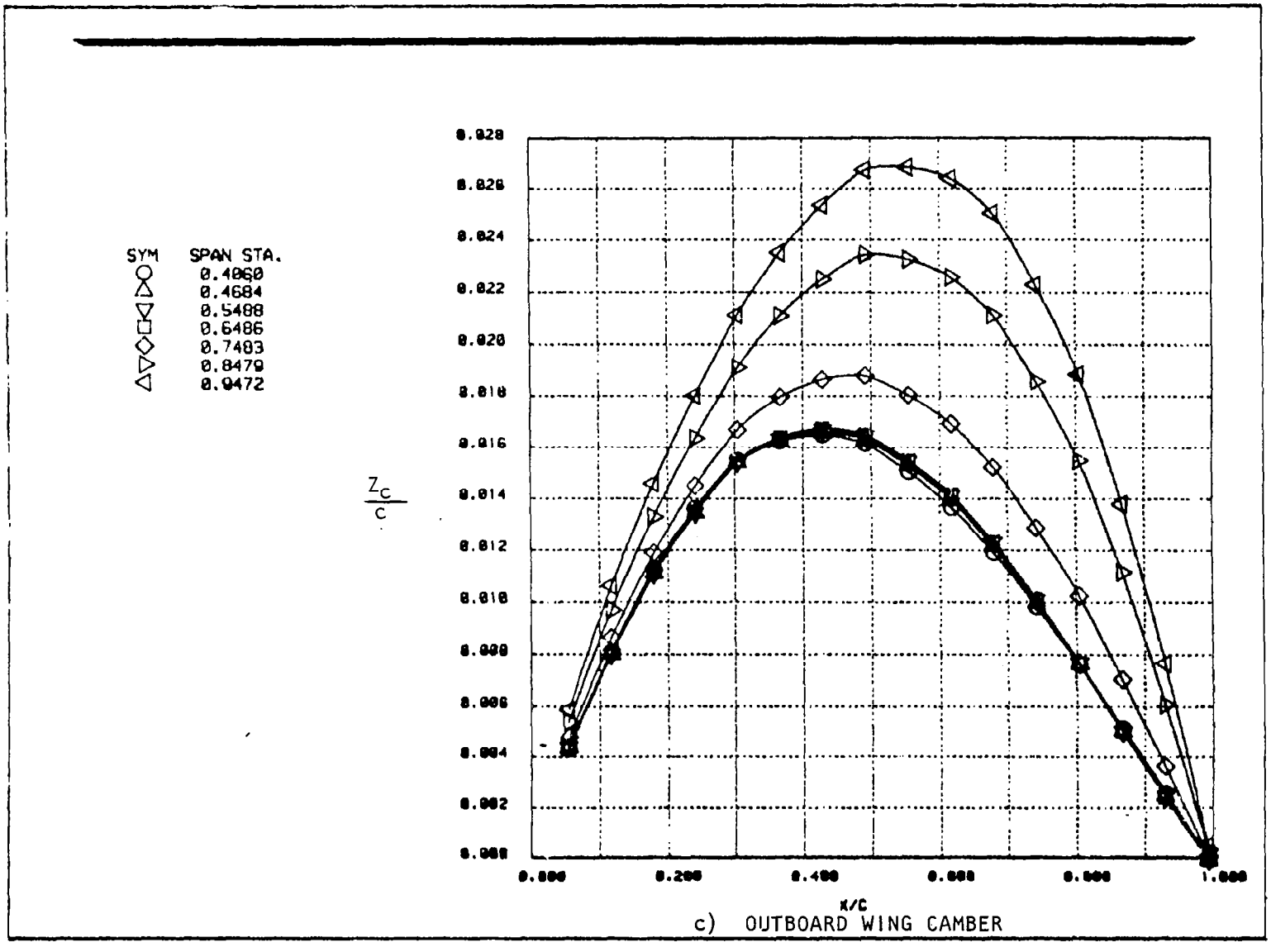

Figure 19. Concluded

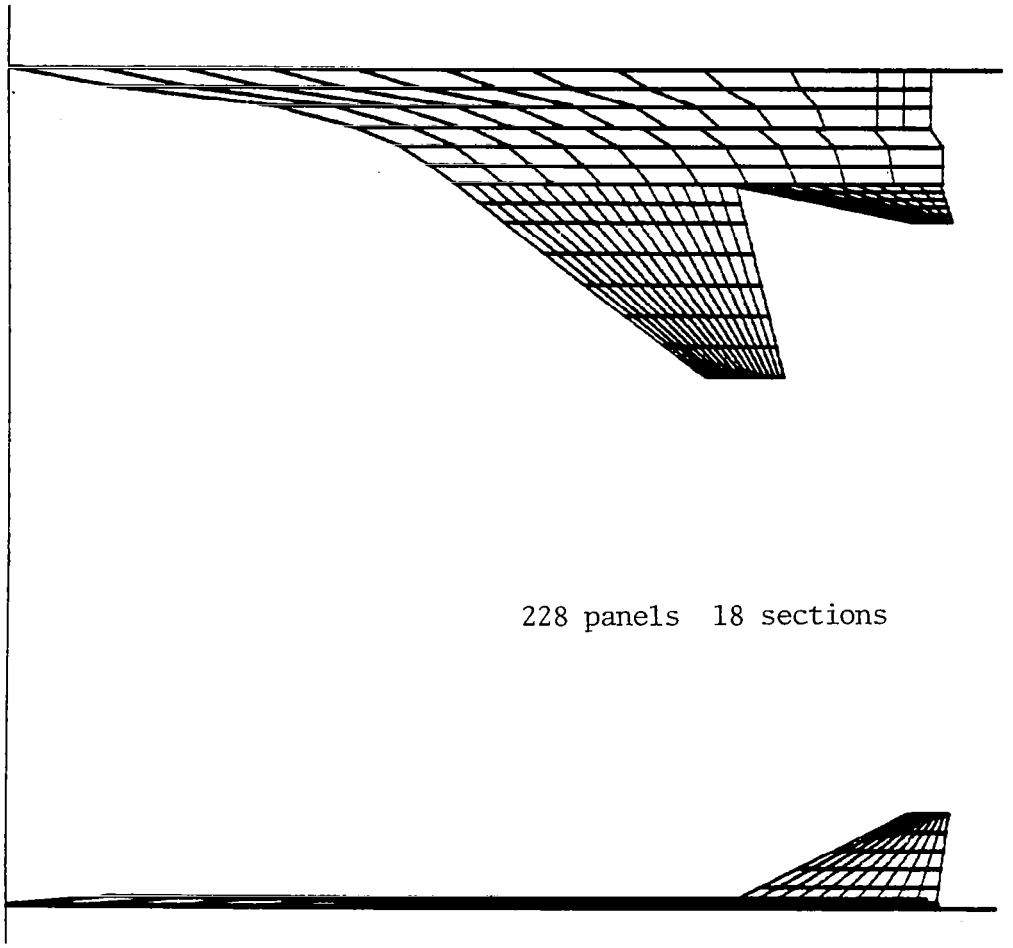

Figure 20. Multipoint Design Linear Theory Finite Element Model

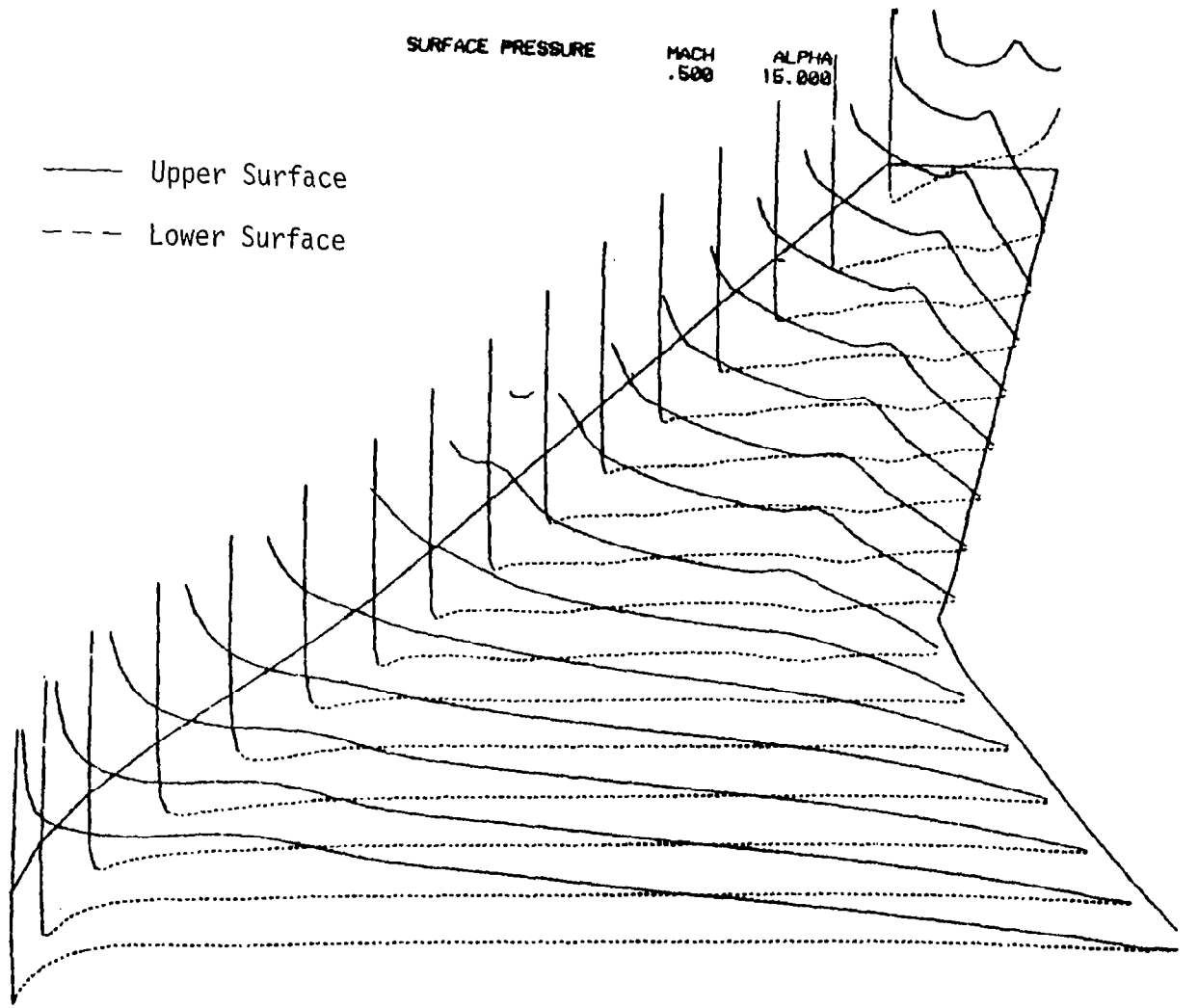

a) Surface pressure isometric

Figure 21. Multipoint Design Subsonic Maneuver Full Potential Analysis
M = 0.5, α = 15 Deg

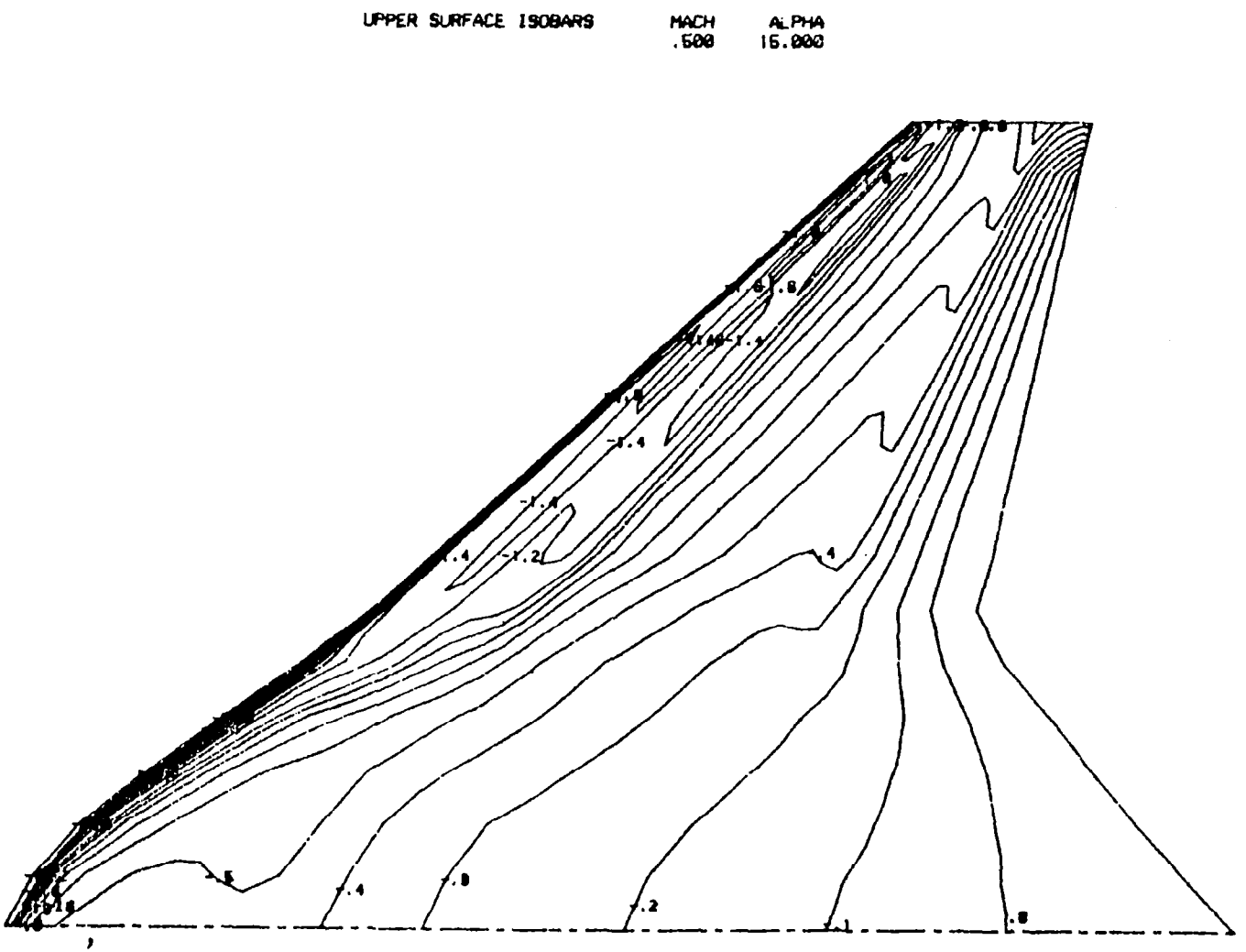

b) Upper surface isobars

Figure 21. Continued

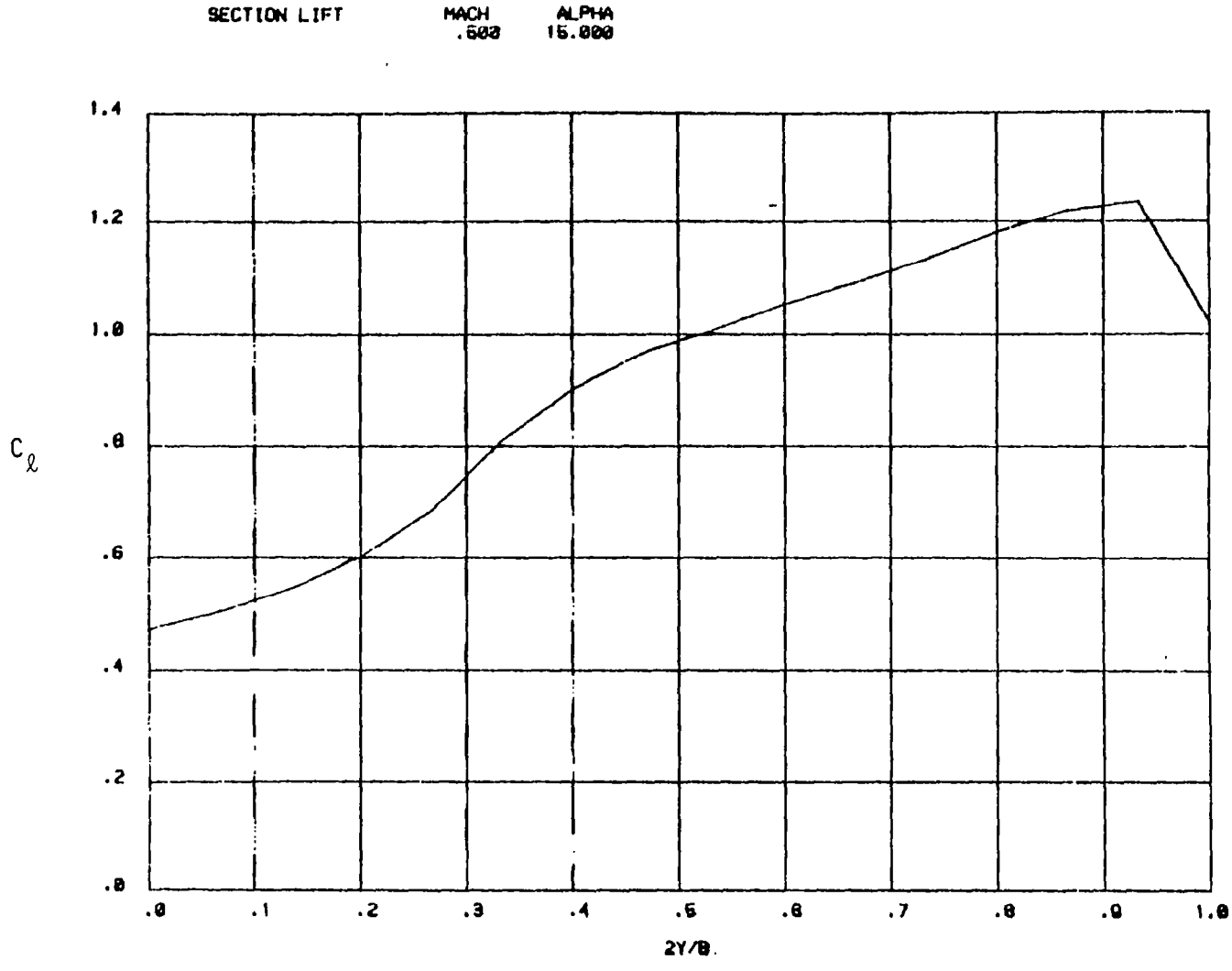

c) Sectional lift

Figure 21. Concluded

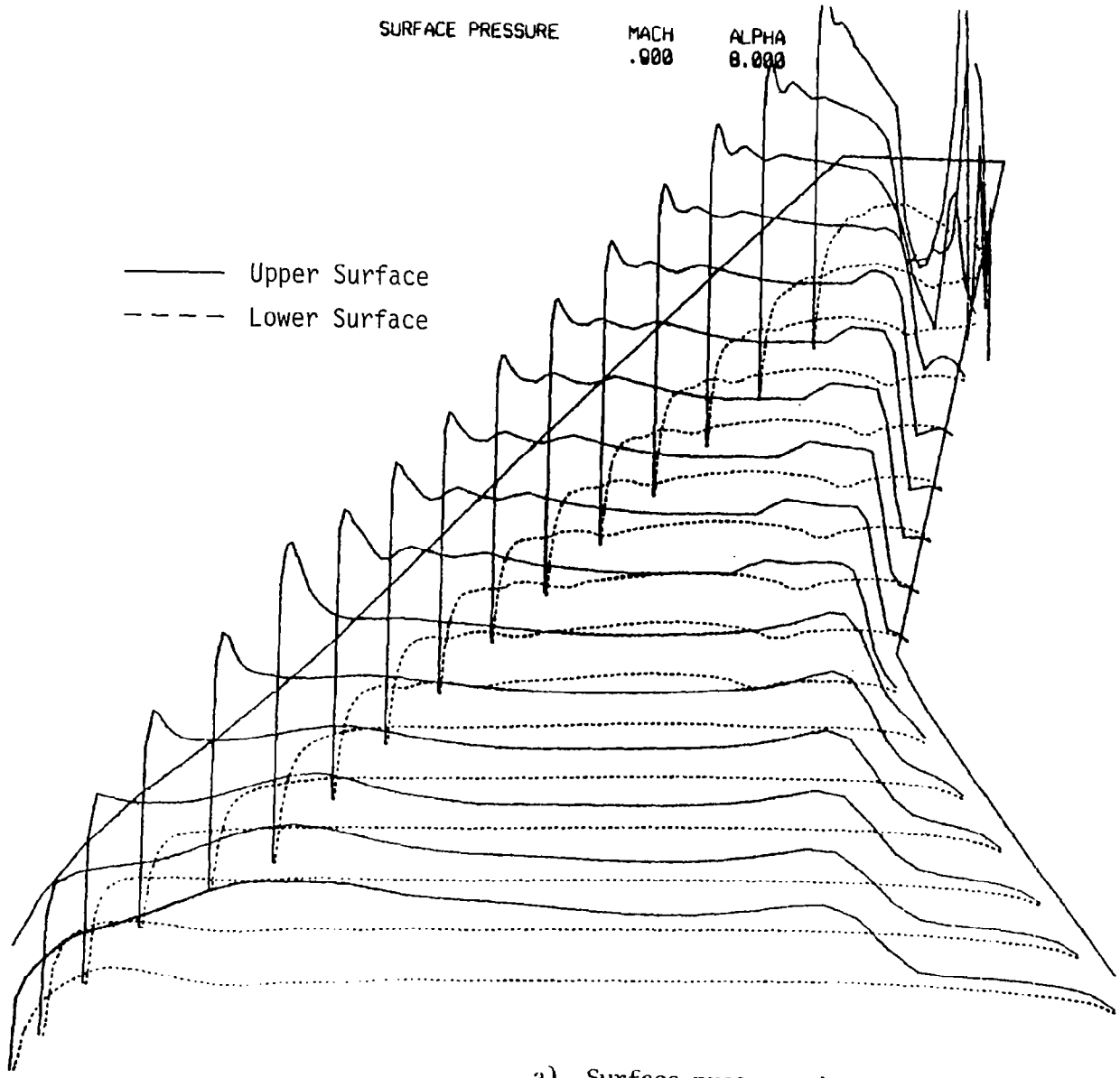

a) Surface pressure isometric

Figure 22. Multipoint Design Transonic Small Disturbance Analysis
M = 0.9, α = 8.0 deg

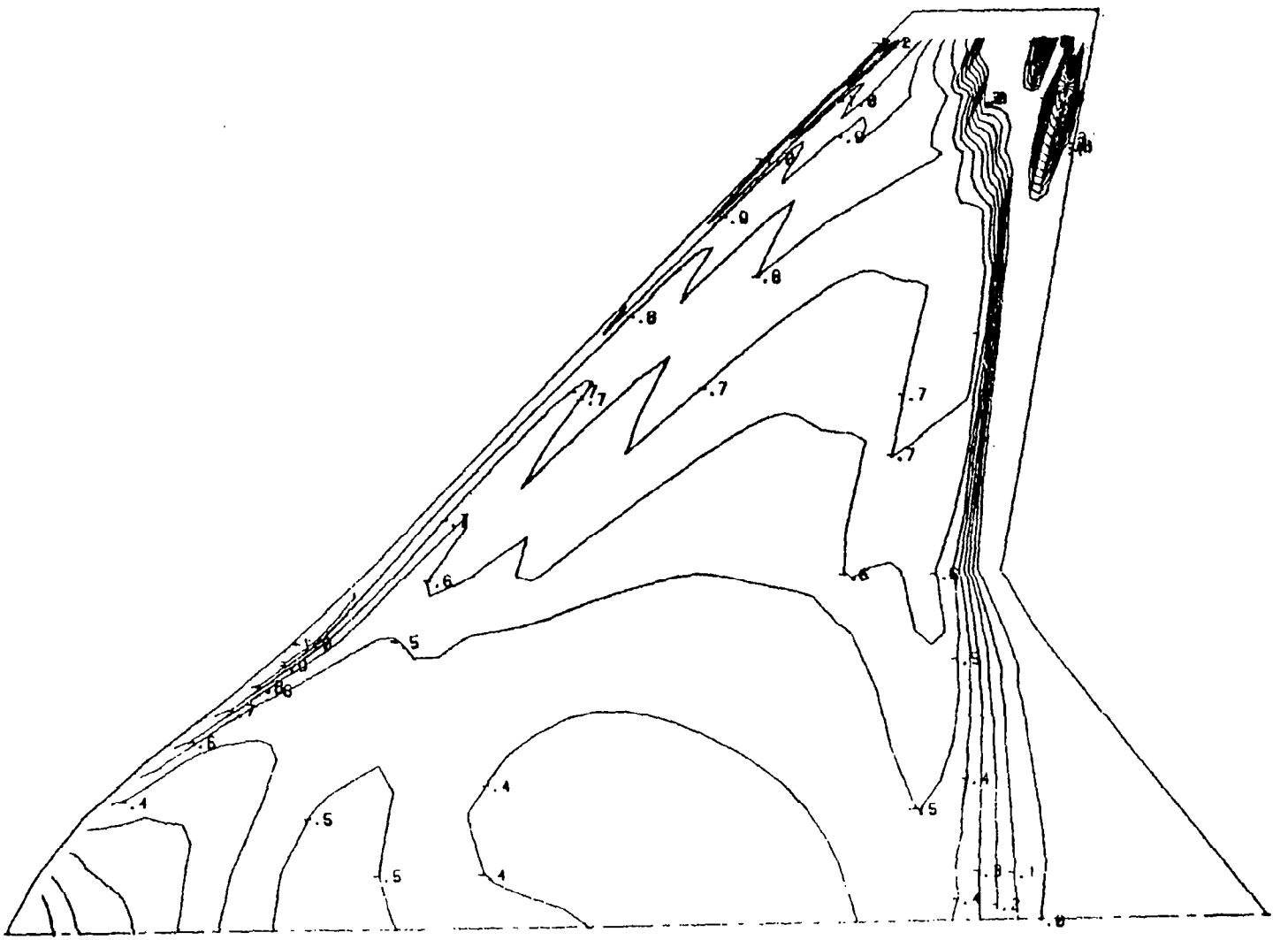

b) Upper surface isobars

Figure 22. Continued

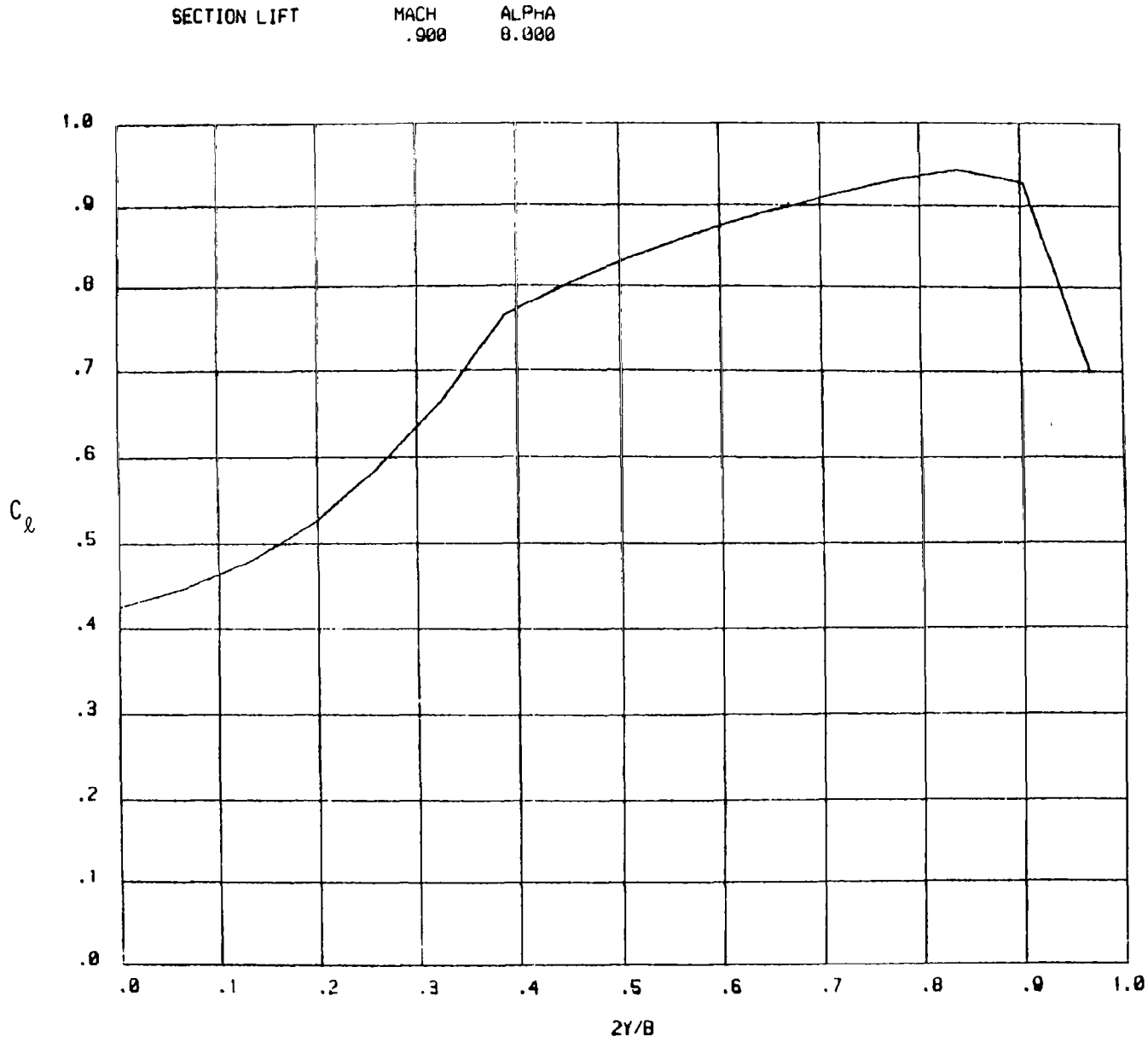

c) Sectional lift

Figure 22. Concluded

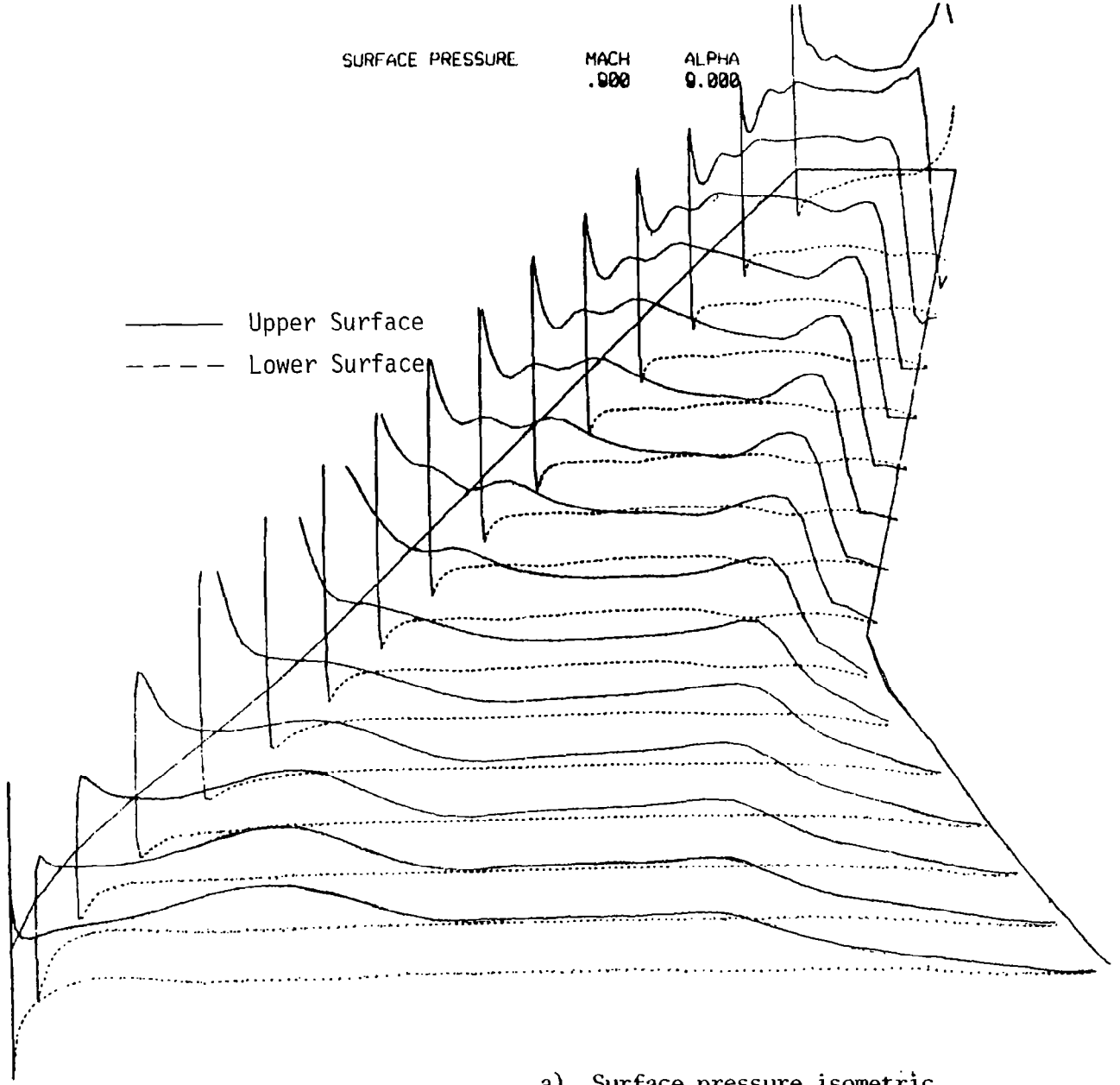

a) Surface pressure isometric

Figure 23. Multipoint Design Transonic Full Potential Analysis
M = 0.9, α = 9.0 deg

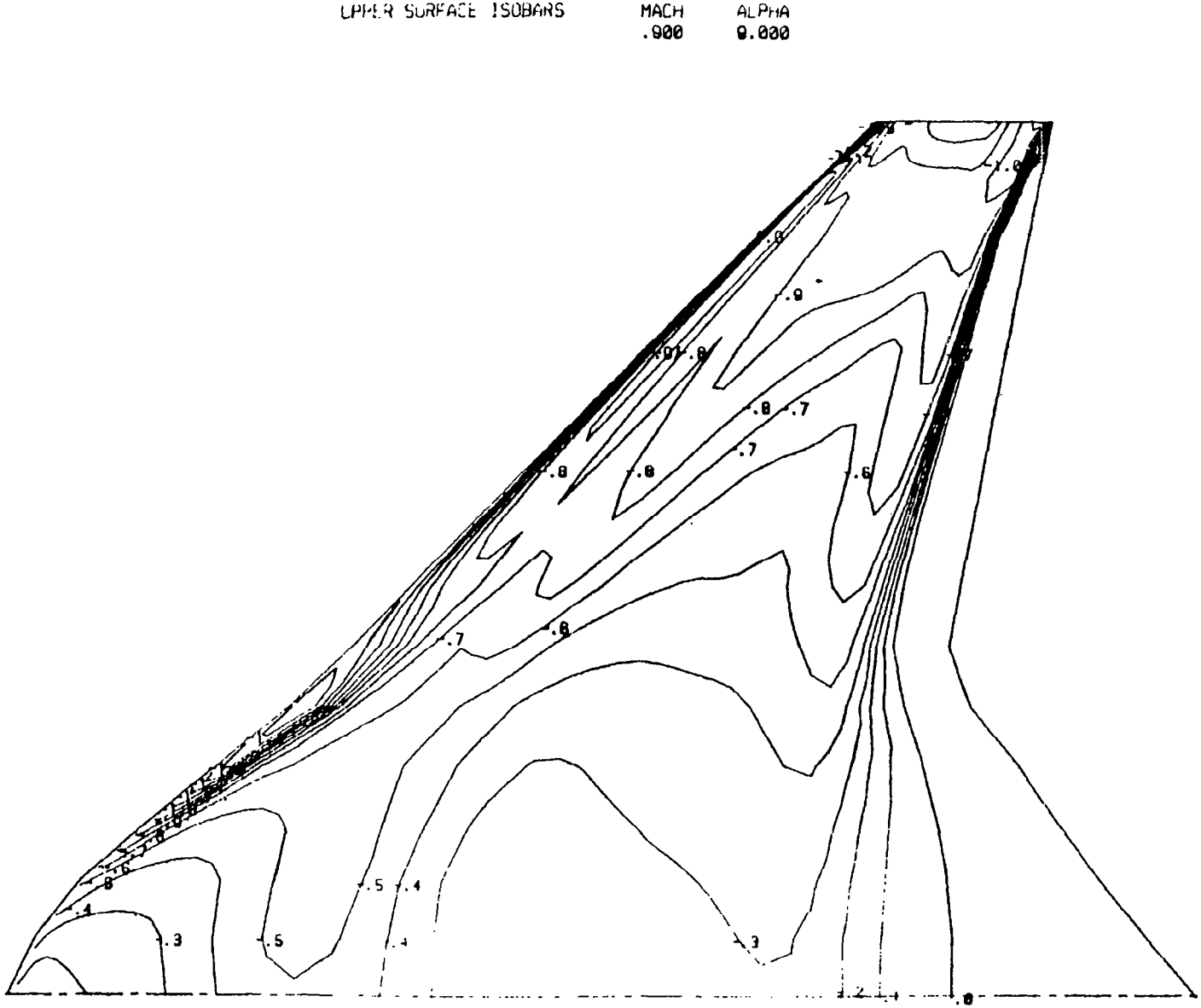

b) Upper surface isobars

Figure 23. Continued

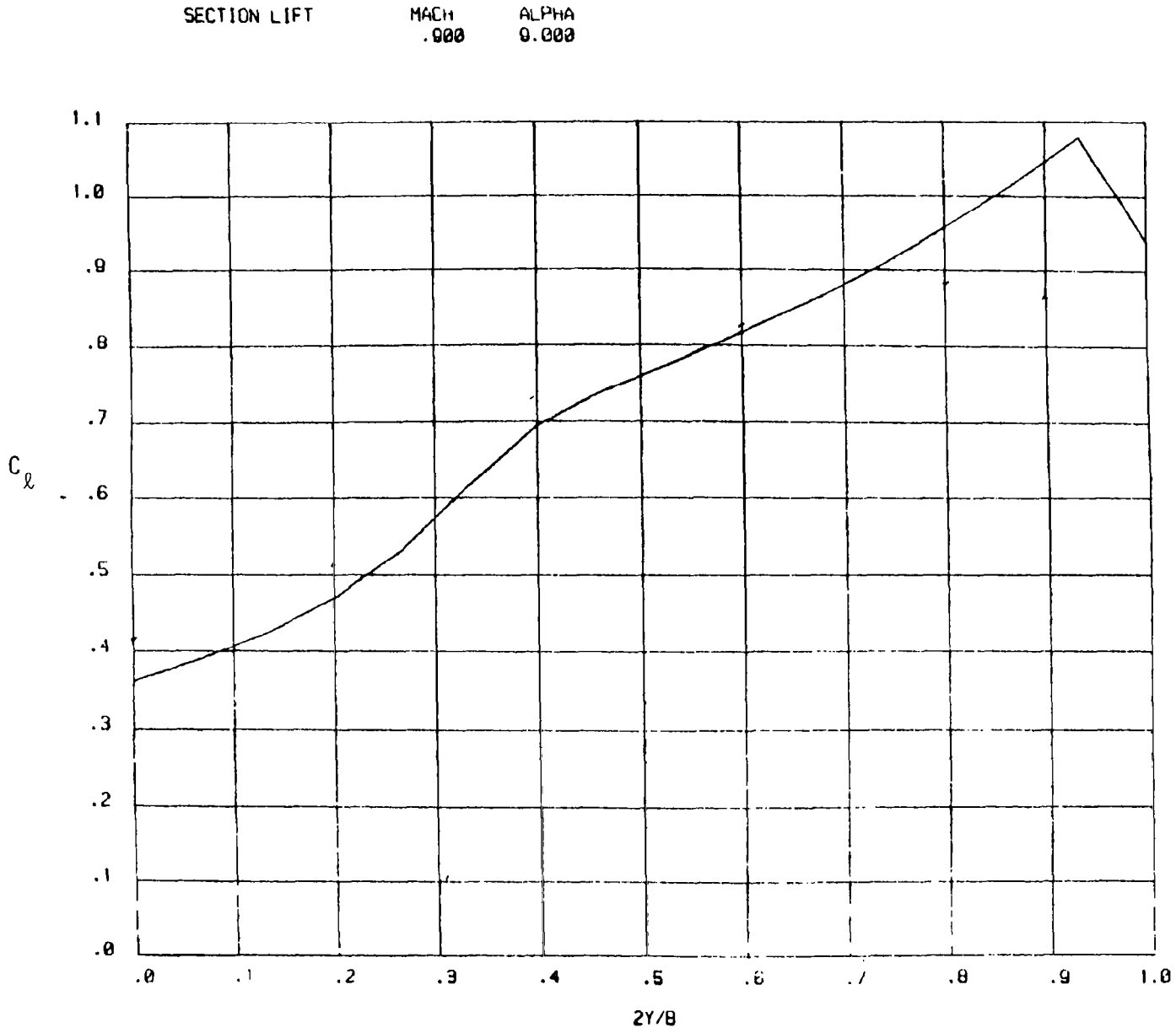

c) Sectional lift

Figure 23. Concluded

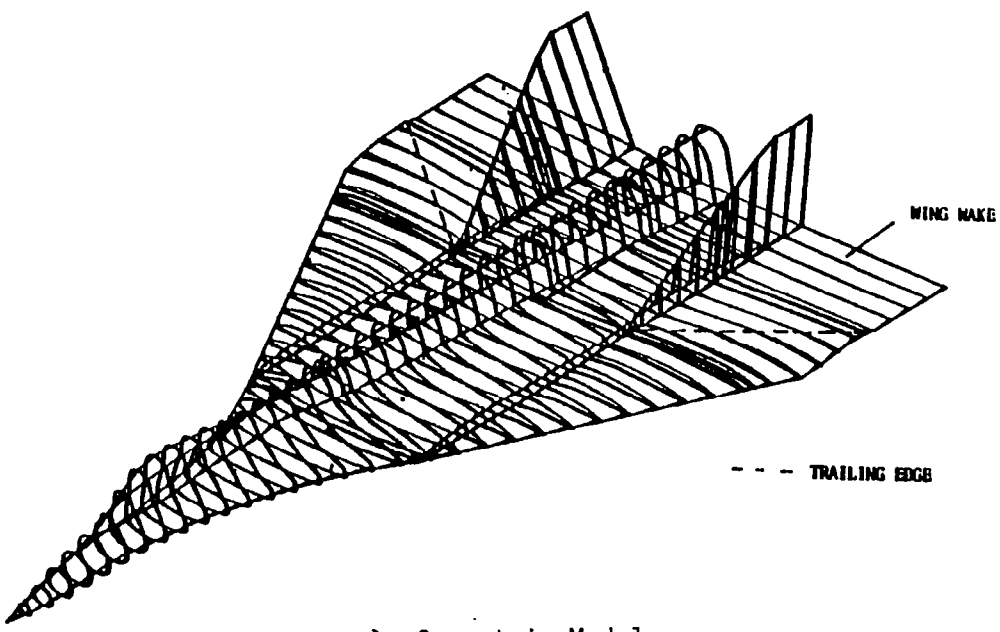

a) Geometric Model

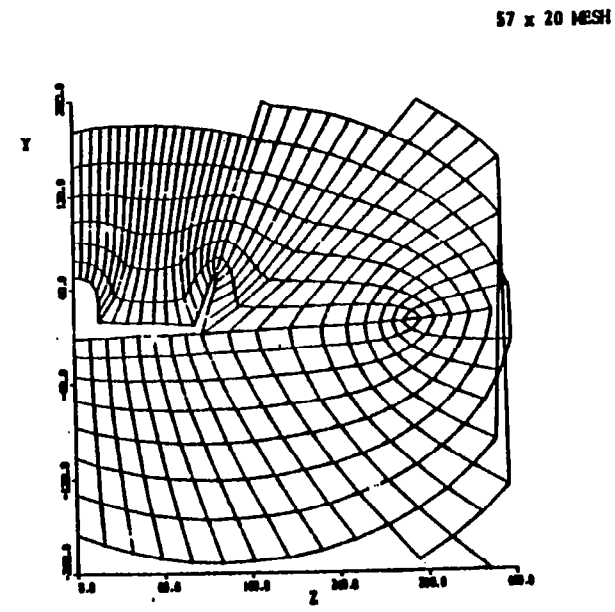

b) Body-Vertical Tail-Wing Wake Grid

Figure 24. Multipoint Design Supersonic Full Potential Analyses

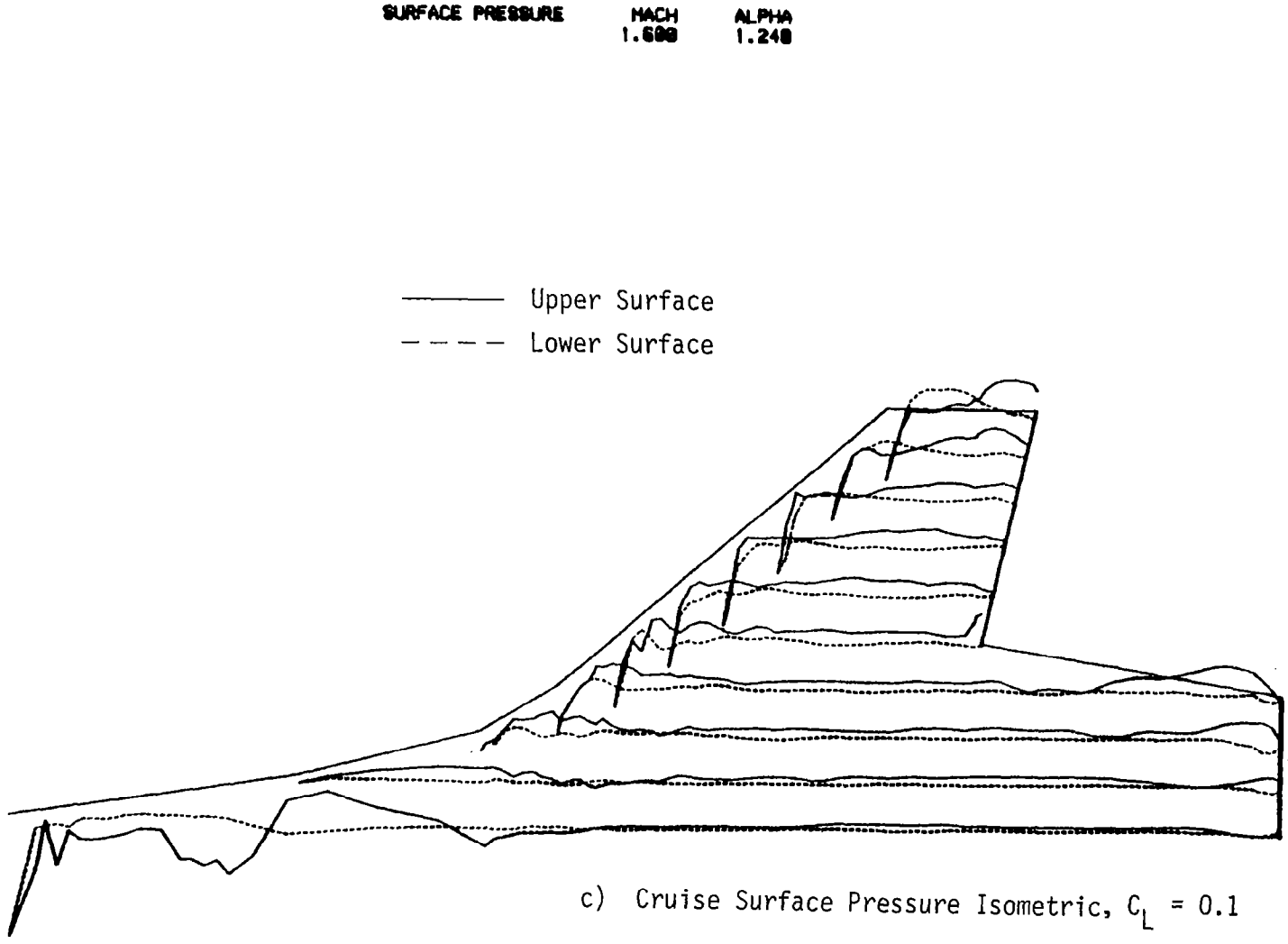

c) Cruise Surface Pressure Isometric, C_L = 0.1

Figure 24. Continued

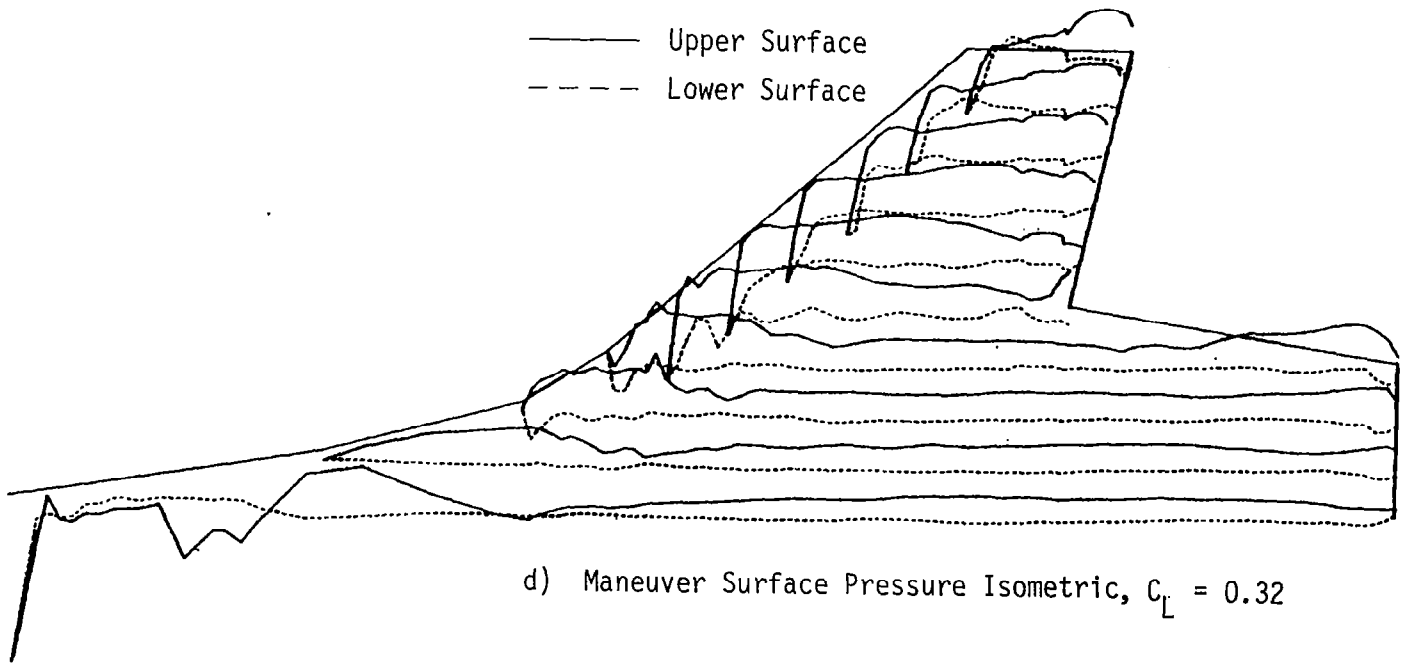

d) Maneuver Surface Pressure Isometric, C_L = 0.32

Figure 24. Concluded

Turbulent Skin Friction

C_{D_F} = 0.0129 at nominal test conditions, $R_{N_{\bar{c}}} = 1.56 \times 10^6$

CRUISE	MANEUVER
Linear Analysis	
α = 1.24 deg	α = 5.22 deg
C_L = 0.1	C_L = 0.32
$C_{D_p} = C_{D_w} + C_{D_L}{}^* = 0.0149 + 0.0031$	$C_{D_p} = C_{D_w} + C_{D_L}{}^* = 0.0149 + 0.0239$
= 0.0180	= 0.0388
C_M = -0.0136	C_M = -0.035
L/D = 3.24	L/D = 6.19
Full Potential	
α = 1.24 deg	α = 5.22 deg
C_L = 0.119	C_L = 0.336
C_{D_p} = 0.0164	C_{D_p} = 0.04075
C_M = -0.0284	C_M = -0.051
L/D = 4.06	L/D = 6.26

*Cambered Plate fuselage

Figure 25. Pretest M = 1.6 Multipoint Design Drag Assessment

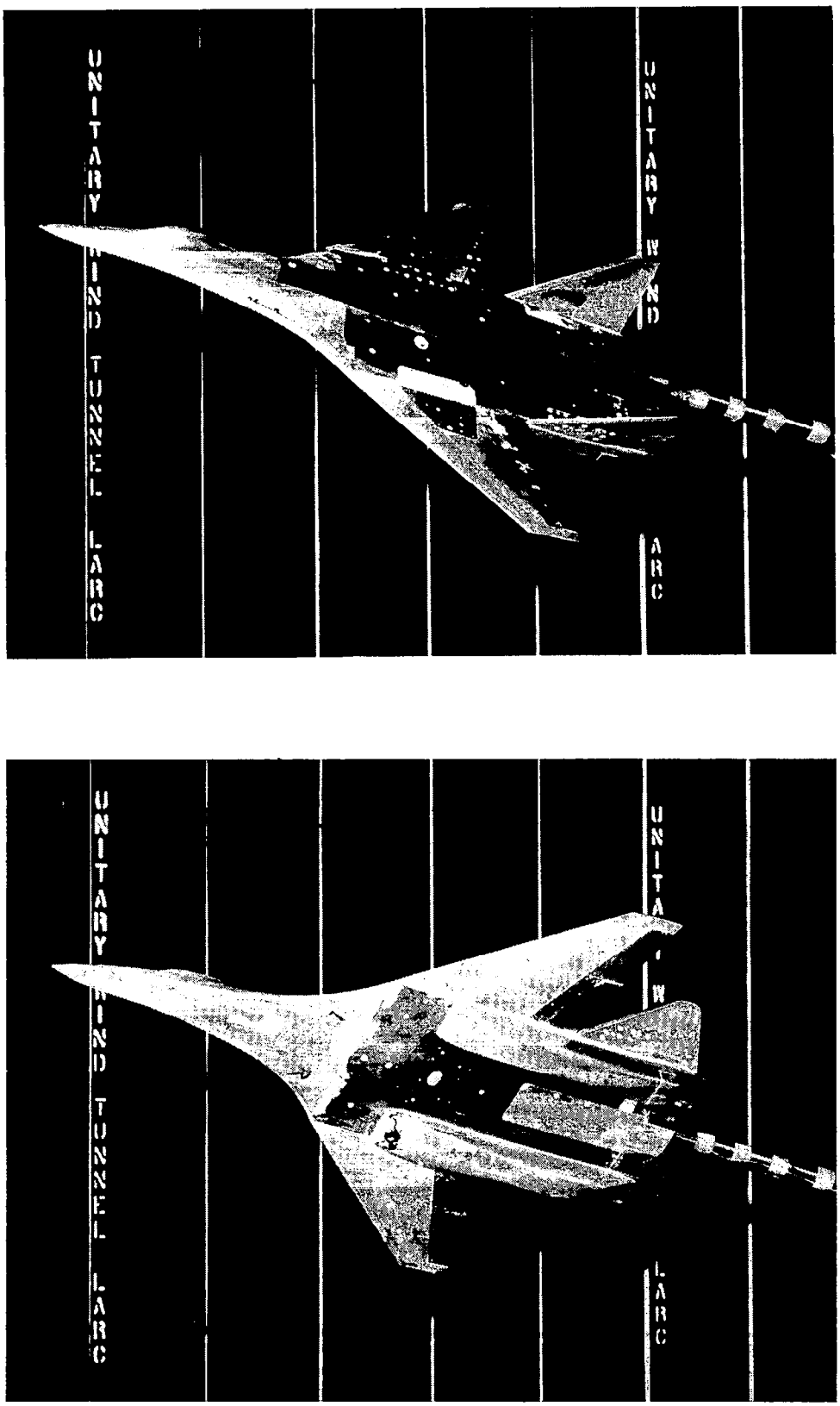

Figure 26. Test Apparatus and Installation

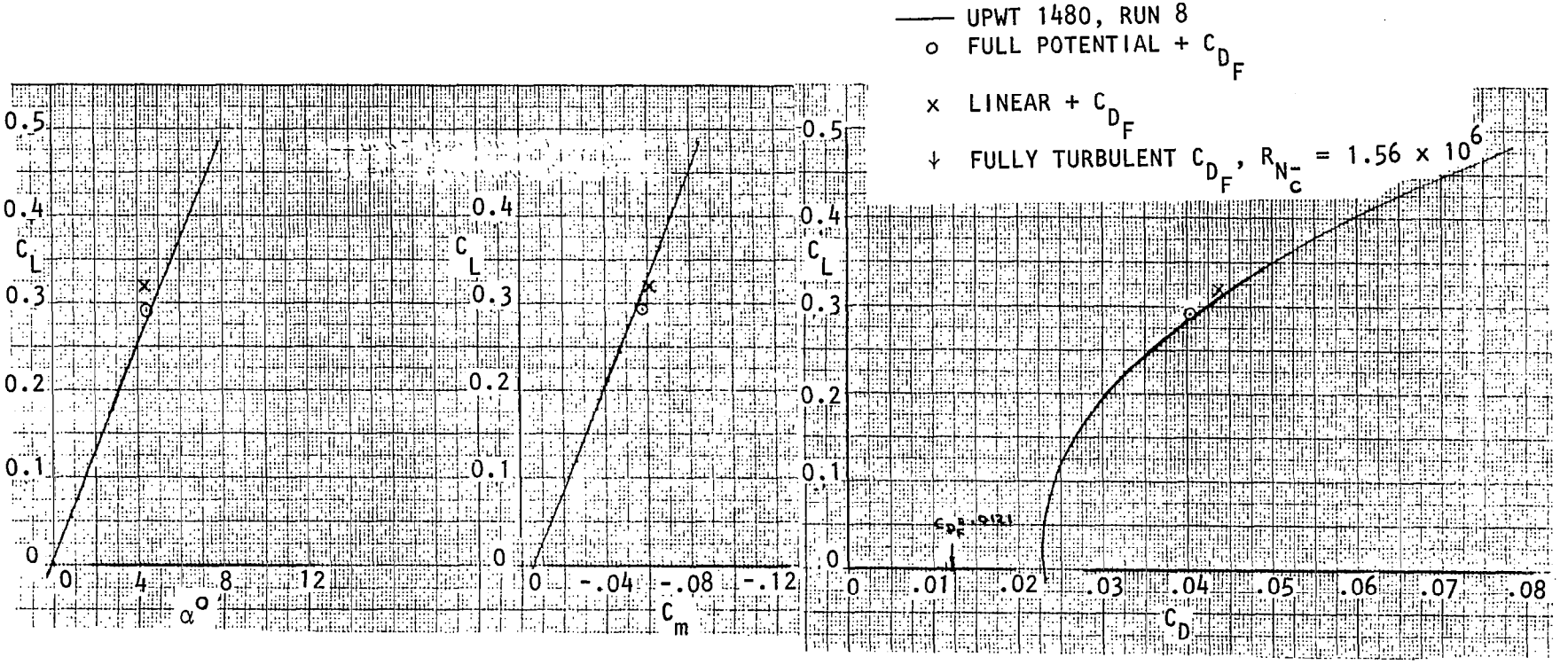

Figure 27. Comparison of Measurement and Predictions at M = 1.6 for Point Design, Nacelle Off

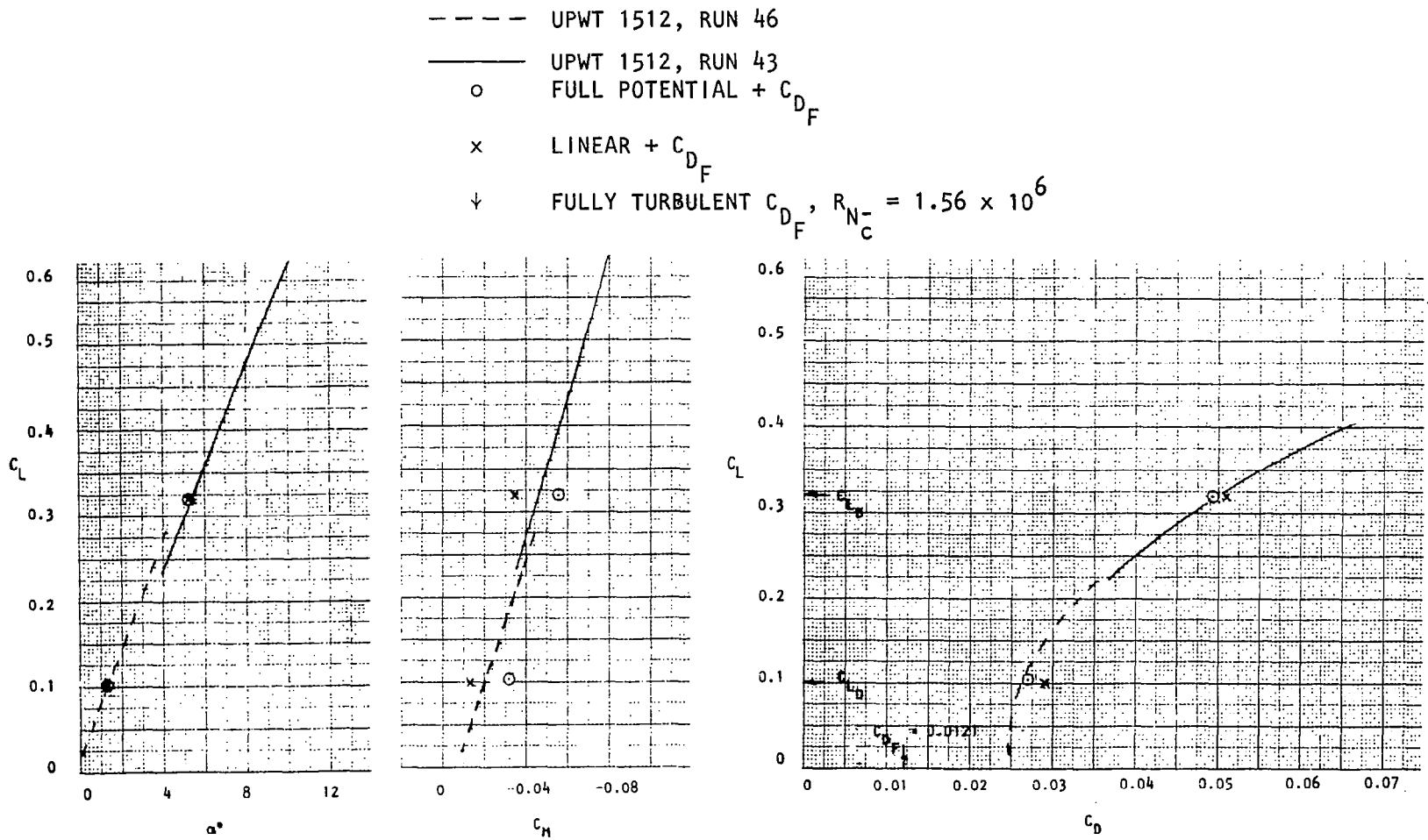

Figure 28. Comparison of Measurement and Prediction at M = 1.6 for Multipoint Design, Nacelle Off

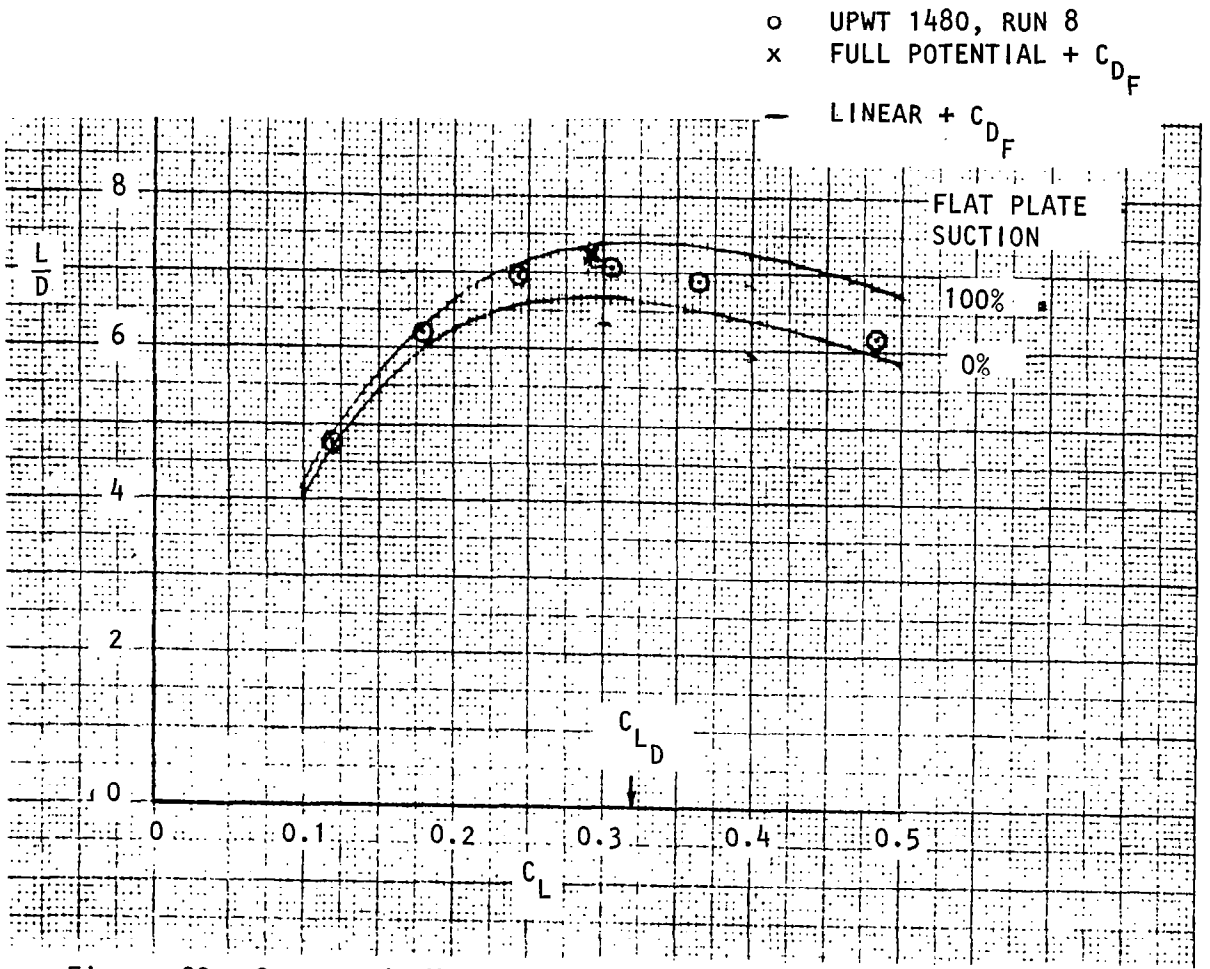

Figure 29. Supersonic Maneuver Point Design Assessment at M = 1.6 Nacelle Off, $R_{N_{\bar{C}}} = 1.56 \times 10^6$

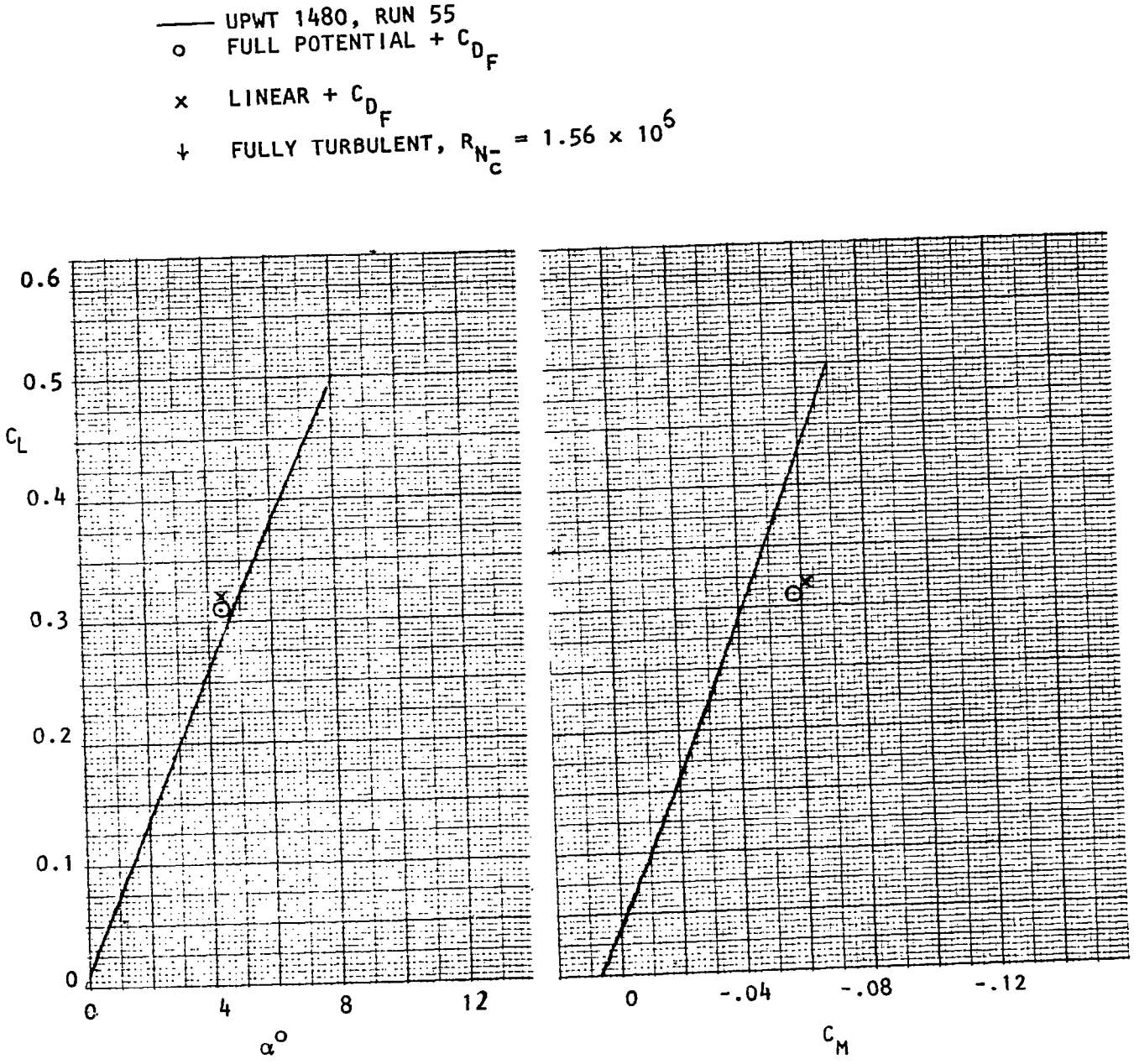

a) LIFT AND PITCHING MOMENT COEFFICIENT

Figure 30. Comparison of Measurement and Predictions at M = 1.6 for the Point Design Wing, Nacelle On

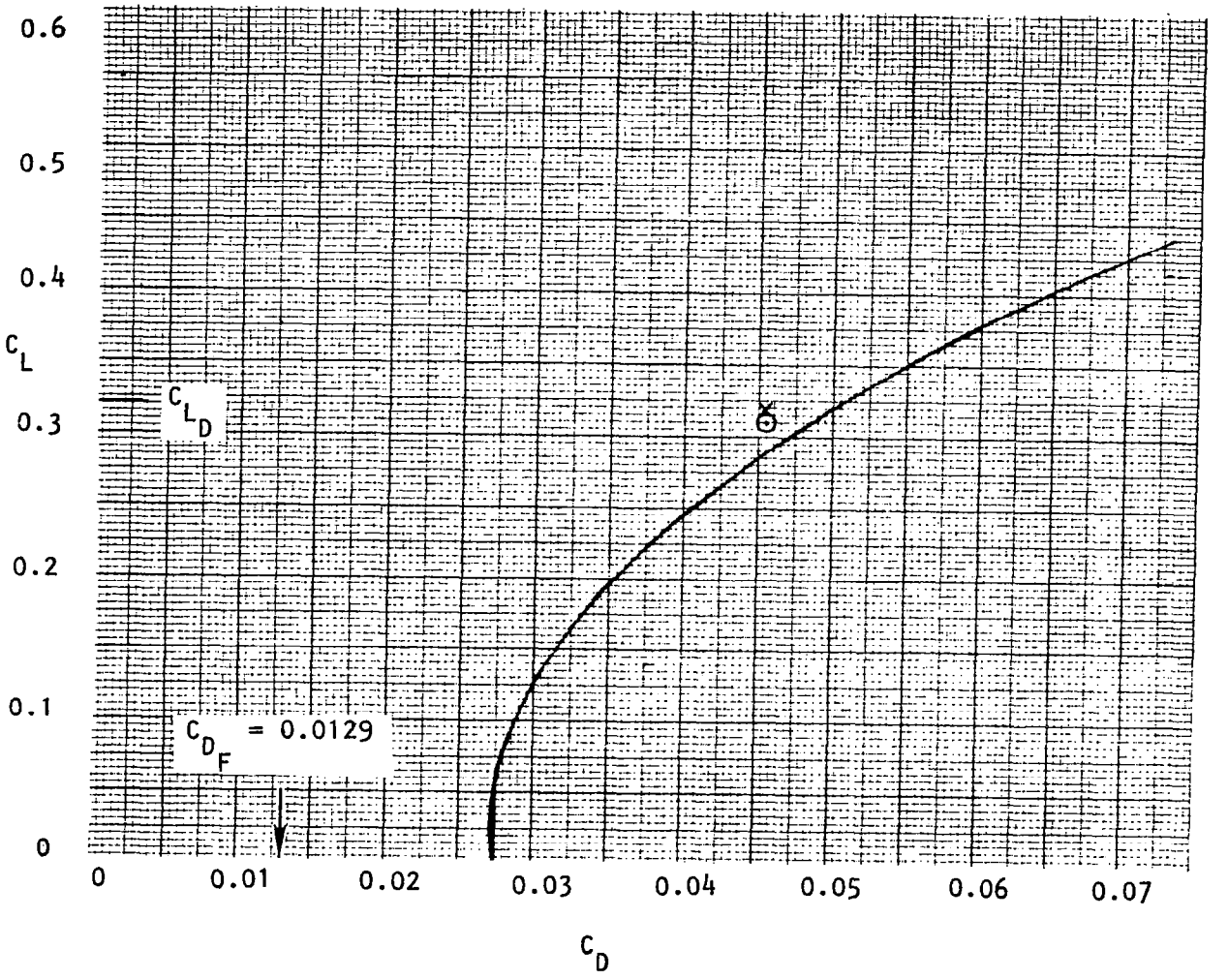

b) DRAG COEFFICIENT

Figure 30. Continued

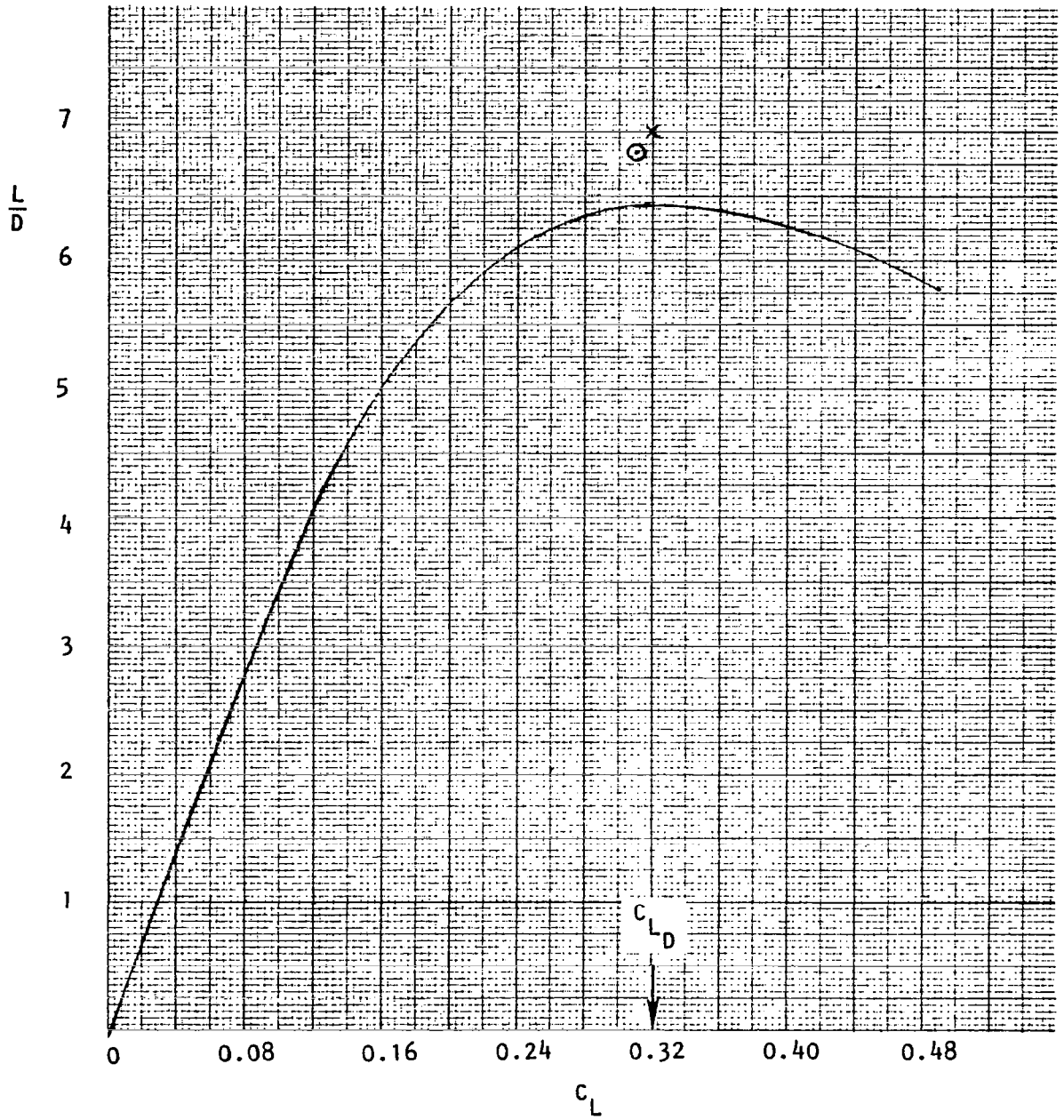

c) LIFT-DRAG RATIO

Figure 30. Concluded

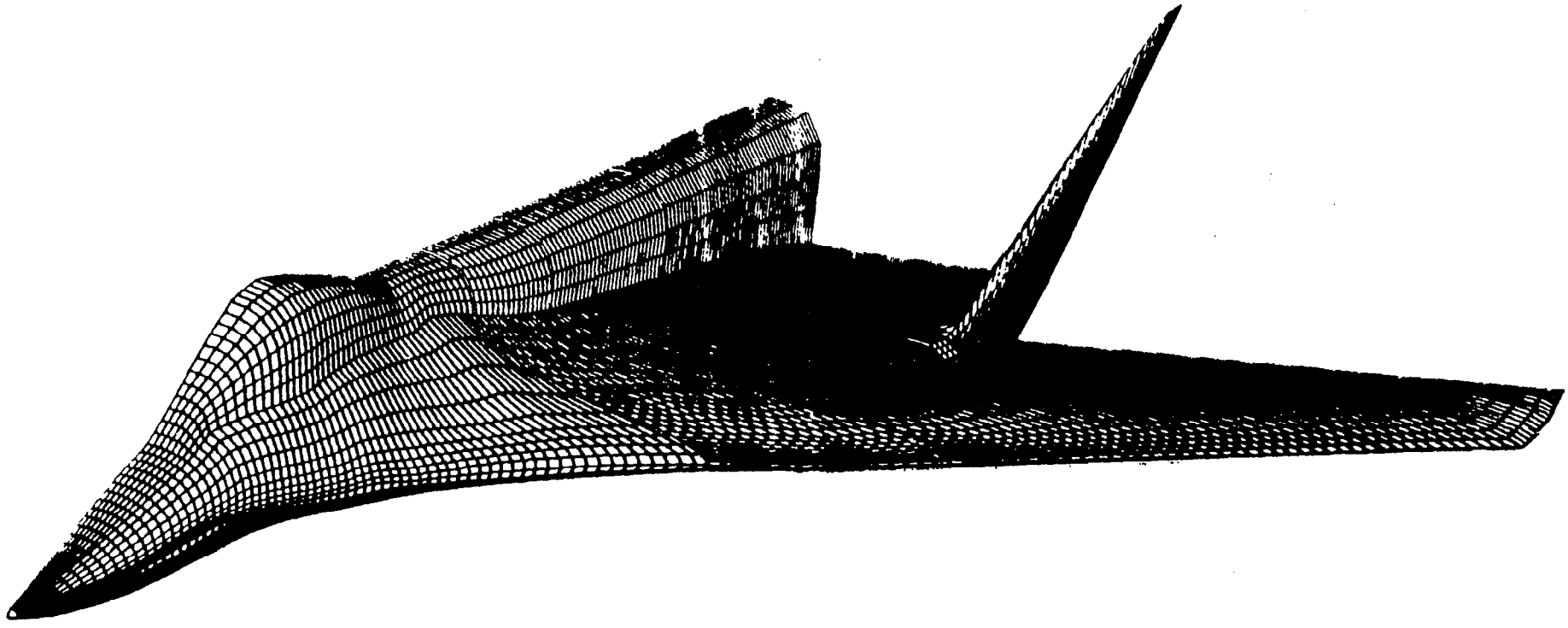

a) TOP VIEW

Figure 31. Point Design Full Potential Surface Grid

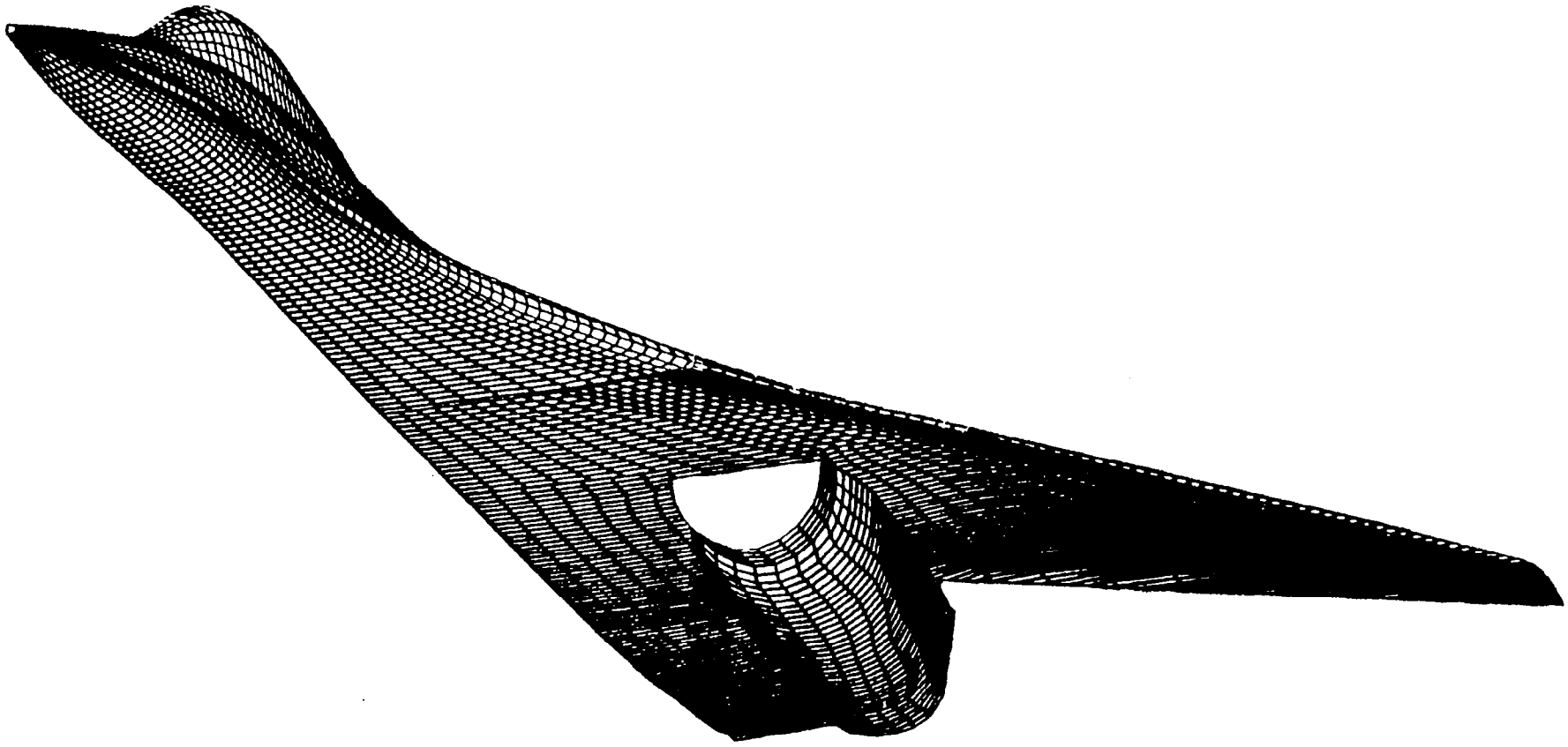

b) BOTTOM VIEW

Figure 31. Concluded

DESIGN	$\Lambda°_{LE}$	TEST	LINEAR	SFP
POINT	55	—UPWT 1480 RUN 8	X	□
SECOND MULTIPOINT	48	--UPWT 1512 RUN 43/46	Y	○

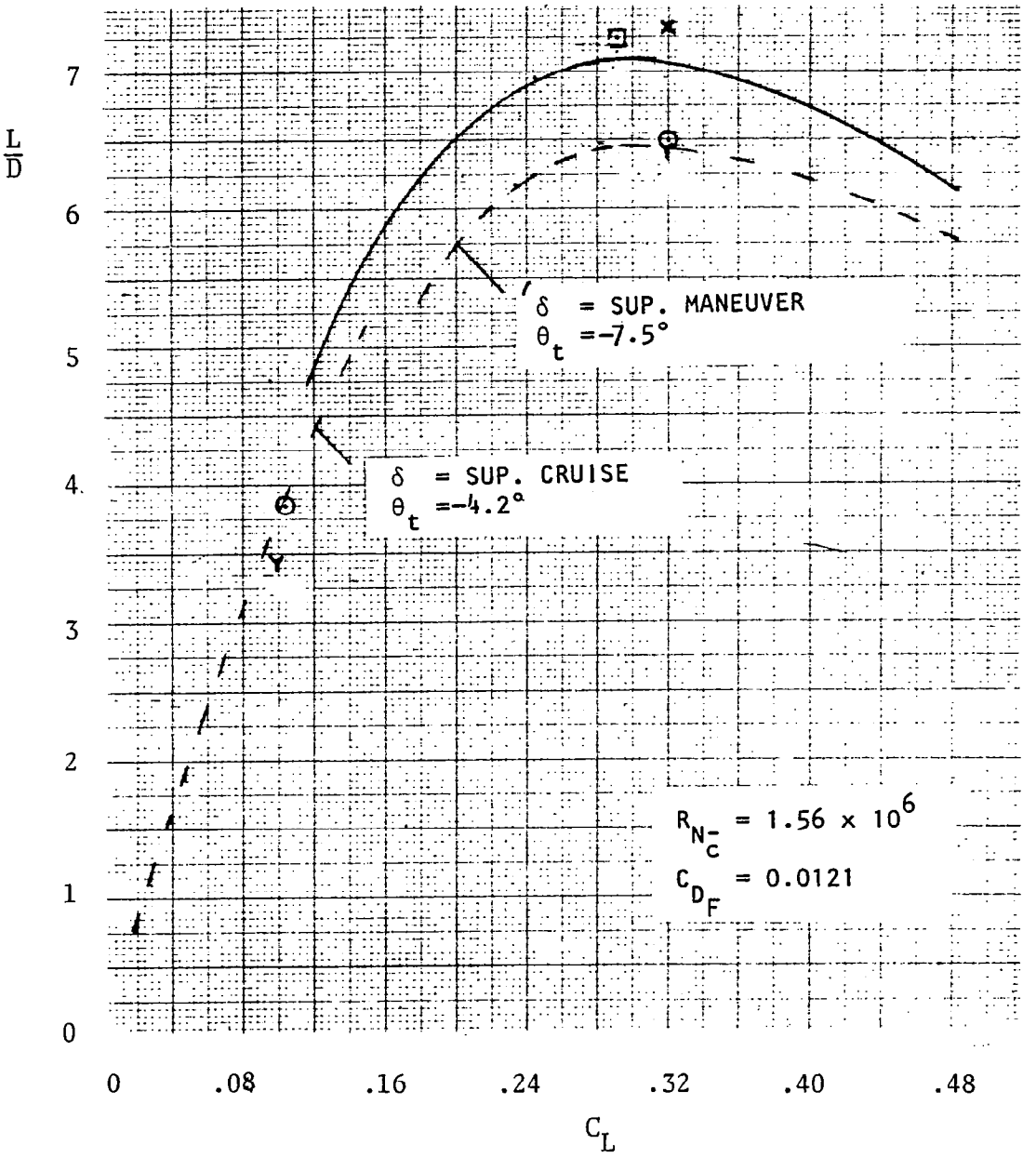

a) NACELLE OFF

Figure 32. Comparison of Point and Multipoint Design Untrimmed Aerodynamic Efficiency at M = 1.6

DESIGN	Λ°_{LE}	TEST	LINEAR	SFP
POINT	55	— UPWT 1480 RUN 55	X	□
SECOND MULTIPOINT	48	--UPWT 1512 RUN 36/52	Y	o

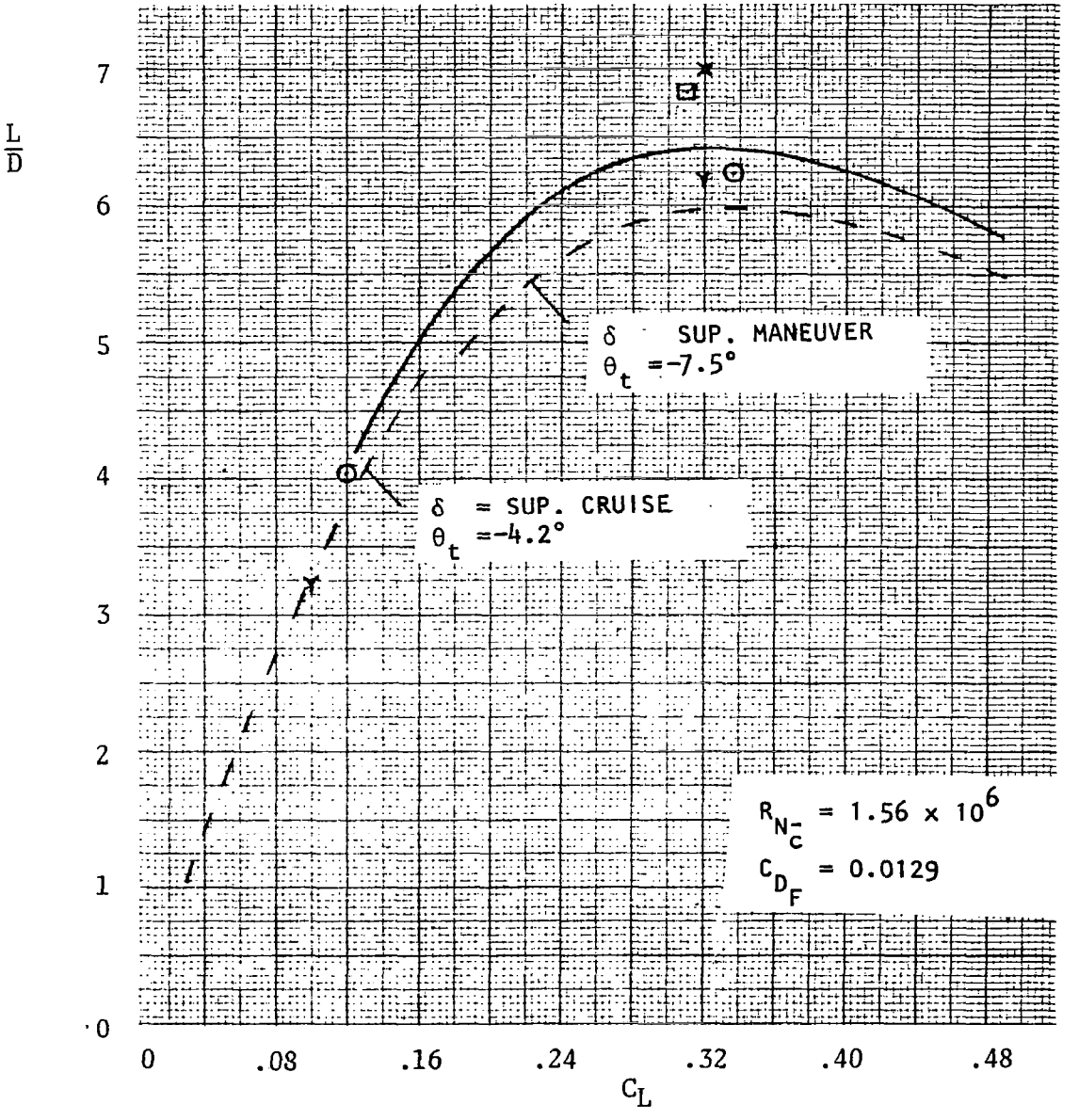

b) NACELLE ON

Figure 32. Concluded

1. Report No.	2. Government Accession No.	3. Recipient's Catalog No.
NASA CR-3950		

4. Title and Subtitle	5. Report Date
Nonlinear Aerodynamic Wing Design	December 1985
	6. Performing Organization Code
7. Author(s)	8. Performing Organization Report No.
Ellwood Bonner	
	10. Work Unit No.
9. Performing Organization Name and Address	
Rockwell International Corporation Los Angeles, California 90009	11. Contract or Grant No. NAS1-15820
	13. Type of Report and Period Covered
12. Sponsoring Agency Name and Address	Contractor Report
National Aeronautics and Space Administration Washington, DC 20546	14. Sponsoring Agency Code 505-43-23-10

15. Supplementary Notes

Langley Technical Monitors: Noel A. Talcott, Jr., and Kenneth M. Jones

Final Report

16. Abstract

The applicability of new nonlinear theoretical techniques is demonstrated for supersonic wing design. The new technology was utilized to define outboard panels for an existing advanced tactical fighter model. Mach 1.6 maneuver point design and multi-operating point compromise surfaces were developed and tested. High aerodynamic efficiency was achieved at the design conditions. A corollary result was that only modest supersonic penalties were incurred to meet multiple aerodynamic requirements. The nonlinear potential analysis of a practical configuration arrangement corrollated well with experimental data.

17. Key Words (Suggested by Author(s))	18. Distribution Statement
Nonlinear Wing Design Potential Theory Supersonic Aerodynamics	LIMITED DISTRIBUTION Until December 1987 Subject Category 02

19. Security Classif. (of this report)	20. Security Classif. (of this page)	21. No. of Pages	22. Price
UNCLASSIFIED	UNCLASSIFIED	80	

NASA-Langley, 1985